MODELING DATA PACKAGE FOR AN INITIAL ASSESSMENT OF CLOSURE FOR C TANK FARM

R. Khaleel
M. P. Connelly
D. Crumpler
T. E. Jones
A. J. Knepp
F. M. Mann
B. McMahon
C. W. Miller
M. I. Wood

CH2M Hill Hanford Group, Inc.
Richland, WA

April 2003

This page is intentionally left blank.

EXECUTIVE SUMMARY

As part of closure of the C tank farm, an initial impact assessment will be conducted to evaluate impacts on groundwater resources (i.e., the concentration of contaminants in groundwater) and long-term risk to human health (associated with groundwater use). The evaluations will consider the extent of contamination from residual wastes in tanks and tank ancillary equipment, past leaks, spills, and retrieval leaks, contaminant movement through the vadose zone to the saturated zone (groundwater), contaminant movement in the groundwater to various locations in groundwater, and the types of assumed human receptor activities at those locations.

This report documents the data that will be used as input to estimate releases from residual wastes in tanks and tank ancillary equipment and to perform flow and transport modeling through the vadose zone and the unconfined aquifer. Contaminant species, representative of long-lived mobile radionuclides, will be considered for flow and transport modeling. All calculations will be performed on the basis of unit inventory and the results based on Tank C-112 will be scaled for the entire C tank farm. A spatial and temporal superposition will be used to obtain a composite contaminant breakthrough curve for releases due to residual wastes in tanks and tank ancillary equipment, past leaks and spills, and retrieval leaks.

This page is intentionally left blank.

CONTENTS

1.0 INTRODUCTION 1
1.1 SCOPE OF THIS DATA PACKAGE 1
2.0 OVERVIEW OF MODELING APPROACH 3
3.0 FACILITY DESCRIPTION AND GEOLOGY 9
4.0 RECHARGE RATES, FLOW AND TRANSPORT PARAMETERS 11
4.1 RECHARGE 11
4.2 FLOW AND TRANSPORT PARAMETERS 13
4.3 STOCHASTIC MODEL FOR MACROSCOPIC ANISOTROPY 14
4.3.1 Macroscopic Anisotropy Parameters 15
4.4 EFFECTIVE TRANSPORT PARAMETERS 15
4.4.1 Bulk Density and K_d 15
4.4.2 Diffusivity 16
4.4.3 Macrodispersivity 16
5.0 GROUNDWATER FLOW AND TRANSPORT 19
5.1 FLOW AND TRANSPORT PARAMETERS 19
6.0 REFERENCES 27

APPENDICES

Appendix A C Tank Farm Closure Numeric Calculations ..... A-i

Appendix B. Advection-, Diffusion-, and Solubility-Dominated Release Models for Residual Wastes ..... B-i

Appendix C. Geologic Cross-Section for C Tank Farm ..... …C-i

Appendix D. C Tank Farm Vadose Zone Flow and Transport Parameter Estimates ..... D-i

FIGURES

Figure 2-1. Overall Modeling Approach for Flow and Transport of Residual Wastes, Past Leaks and Retrieval Leaks 5
Figure 3-1. C Tank Farm and Surrounding Facilities. 9
Figure 5-1. VAM3D-generated steady state hydraulic head (m) distribution for the Hanford Site for post-Hanford conditions (after Lu 1996). 20
Figure 5-2. VAM3D-Generated Pathline Distribution at Steady State for Post-Hanford Conditions (after Lu 1996). 21
Figure 5-3. Material Property Distribution for the Upper Three Elemental Layers for VAM3D Sitewide Groundwater Model (after Law et al. 1996). 22

TABLES

Table 4-1. C-106 Infiltration (Recharge) Estimates for Pre-Construction Period, Current Conditions, and Following Emplacement of Closure Barrier.....13

Table 4-2. Composite Van Genuchten-Mualem Parameters for Various Strata.....13

Table 4-3. Macroscopic Anisotropy Parameters, Based on Polmann (1990) Equations (Appendix D) for Various Strata. 15

Table 4-4. Effective Parameter Estimates, $E[P_bK_d]$, for U For the Product of Bulk Density (g/cm^3) and K_d (cm^3/g).....16

Table 4-5. Non-Reactive Macrodispersivity Estimates for Various Strata. 17

Table 5-1. Hydraulic Properties for Various Material Types for Sitewide Vam3D Groundwater Model (after Law et al. 1996). 24

Table 5-2. Transport Parameters for the Site-Wide Groundwater Model. 25

LIST OF TERMS

BTC	breakthrough curve
DMT	Data Management Tool
DST	double-shell tanks
Ecology	Washington State Department of Ecology
FLTF	Field Lysimeter Test Facility
ILAW	Immobilized Low-Activity Waste
PA	Performance Assessment
PTB	Prototype Hanford Barrier
RCRA	Resource, Conservation, and Recovery Act
SST	single-shell tanks
WAC	Washington Administrative Code
WMA	waste management area

1.0 INTRODUCTION

Under the Tri-Party Agreement, both single-shell tanks (SST) and double-shell tanks (DST) are Resource, Conservation, and Recovery Act (RCRA) hazardous waste management units that will eventually be closed under *Washington Administrative Code* (WAC) 173-303, "Dangerous Waste Regulations." Three options exist for the closure: 1) clean closure, involving removal of all waste and waste constituents, including tank, debris, contaminated equipment, and contaminated soil and groundwater; 2) modified closure, which involves a variety of closure methods but requires periodic (at least once after 5 years) assessments to determine if modified closure requirements are being met; and 3) closure as a landfill with waste remaining in-place and corrective action taken for contaminated media under post-closure requirements. All three options require the submittal of closure plans and their approval by Washington State Department of Ecology (Ecology). The objective of this report is to document the data that will be used as input to perform preliminary flow and transport modeling through the vadose zone and the unconfined aquifer for closure of the C tank farm in 200 East Area. Calculations will be performed based on unit inventory for various contaminant source terms, and the modeling results based on Tank C-112 will be scaled for other tanks in the C tank farm. For the purpose of this initial assessment, it is assumed that the C tank farm will ultimately be closed as a landfill.

1.1 SCOPE OF THIS DATA PACKAGE

The following information is included as part of the scope for this data package for the modeling:

- Modeling approach (Section 2.0).
- Source-term release scenarios for release of residual waste contaminants from tanks and tank ancillary equipment (Appendix B).
- Facility description and stratigraphic cross-sectional model for the C tank farm (Section 3.0 and Appendix C).
- Recharge (infiltration) data for C tank farm (Section 4.0).
- Effective (upscaled) moisture retention, saturated and unsaturated hydraulic conductivity, bulk density, diffusivity, and macrodispersivity estimates for various strata (Section 4.0 and Appendix D).
- Macrodispersivity estimates for selected radionuclide species (Section 4.0 and Appendix D).
- Groundwater flow and transport parameters (Section 5.0).
- Numerical cases to be run (Appendix A).

This page is intentionally left blank.

2.0 OVERVIEW OF MODELING APPROACH

The source terms for the initial assessment consist of four separate sources that include (a) past leaks and spills, (b) leakage during retrieval, (c) residual waste leachate from tanks following closure, and (d) residual waste leachate from tank ancillary equipment following closure. The past leaks represent tank waste that has leaked into the vadose zone and has been migrating through the vadose zone for a number of years. Retrieval leakage refers to leakage to vadose zone that could occur during waste retrieval operations using water-based sluicing. Releases from the residual wastes (both from tank and tank ancillary equipment) would typically occur over an extended period following closure of the tank farm when infiltrating water would enter the tank or tank ancillary equipment, dissolve contaminants, and migrate into the vadose zone and to the groundwater.

The overall modeling approach is illustrated in Figure 2-1. The dominant pathway is through groundwater, as indicated by previous Hanford Site performance assessments and environmental impact statements. Following closure, it is assumed that infiltration of moisture from precipitation eventually enters the tank facility, mixes with the post-retrieval residual wastes; the moisture causes the contaminants to be released into the vadose zone from the degraded tank structure. The released contaminants then travel through the vadose zone where they meet and mix with already-released contaminants, if any, from past leaks, spills, and retrieval. The contaminants travel through the vadose zone until they reach the water table and the unconfined aquifer. The contaminant breakthrough curves (BTC) from residual wastes, past leaks and retrieval for all tanks in C tank farm are combined via a spatial and temporal superposition. The combined BTCs are then routed to various locations within the unconfined aquifer and the Columbia River, using an analytical solution (i.e., streamtube model).

The two-dimensional simulations yield the contaminant mass flux and BTCs at the tank farm fence line along the tank centerlines for the selected cross-section. The tank centerline mass flux and BTCs are transformed to average values across the tank farm fence line using two translations (*FY00 Initial Assessments for S-SX Field Investigation Report (FIR): Simulations of Contaminant Migration with Surface Barriers,* White et al. 2001). In the first translation, the centerline quantities are converted to average quantities on the tank farm fence line boundary as the cross-sectional projections. The length of the cross-sectional projection equals the mean inventory diameter, where the mean inventory diameter is computed for each source inventory. Note that the inventory diameter is not necessarily the tank diameter. In the second translation, the cross-sectional average mass flux or BTCs for various cross-sections are translated to a single average mass flux or BTC across the entire tank farm fence line length using a length-weighted averaging scheme (White et al. 2001).

All calculations are for Tank C-112 and for unit Curie (or unit mass) as a source term for each of the four sources (i.e., past leaks and spills, retrieval, residual tank wastes and ancillary equipment). For residual tank wastes and residual ancillary equipment wastes, actual release mechanisms are unknown. For an accurate determination of the source term, the chemical and physical processes controlling contaminant release from the residual wastes must be explicitly modeled. In the absence of post-retrieval tank waste characterization data and a lack of

knowledge of the controlling processes, a series of scenarios are assumed for contaminant release
from tank wastes and tank ancillary equipment such that the modeling results cover a range of potential outcomes.

One set of release scenarios assumes that the release rates from residual wastes are directly proportional to recharge (infiltration) rates and the release durations vary with durations of varying recharge rates. This essentially results in uniform release rates over specified release periods, with the unit source released over the entire release duration. A similar approach has been used in various versions of the *Immobilized Low-Activity Tank Waste* (ILAW) *Performance Assessment* (PA) (e.g., Mann et al. 2001). The other set of release scenarios let the release duration vary based on various controlling processes (i.e., advection, diffusion, or solubility) that are active during release from residual wastes. In addition to recharge (infiltration) rates, these models consider the mixing (advection and diffusion) processes (Appendix B) occurring within the residual wastes. A similar approach has been recommended by the U.S. Nuclear Regulatory Commission for the low-level waste PA (*Background Information for the Development of a Low-Level Waste Performance Assessment Methodology,* Kozak et al. 1990) and has been used for the *Performance Assessment for the Disposal of Low-Level Waste in the 200 West Area Burial Ground* (Wood et al. 1995), and the *Performance Assessment for the Disposal of Low-Level Waste in the 200 East Area Burial Grounds at the Hanford Site* (Wood et al. 1996). The radionuclides considered for the advection-, diffusion-, and solubility-dominated process models for release from residual wastes are Tc-99, I-129 and U. Details are presented later (see Appendix A and Appendix B).

For some of the first set of scenarios, because of the assumed slow release of contaminants from the residual wastes, the expected BTCs in the groundwater are expected to show a relative broadening of the peak concentration rather than show a sharp peak. This contrasts with the expected BTCs for the second set of scenarios, where the contaminant release time is relatively short compared to the contaminant travel time through the vadose zone, resulting in a much sharper peaked response. In any case, the two sets of scenarios for release from residual wastes in tanks and tank ancillary equipment are chosen to produce a range of potential outcomes.

In contrast to releases from residual wastes in tanks and tank ancillary equipment, releases from the past leaks, spills, and retrieval occur over a much shorter period. The retrieval case simulations will assume that a unit source is lost at specified leak volumes at the bottom of the tank over a 5-ft wide annulus at the outer right edge of the tank (*Description of Vadose Zone/Groundwater Flow and Transport Numerical Modeling for S Tank Farm Retrieval Performance Evaluation,*Williams et al. 2001). The simulations for past leaks and spills will not attempt to model a waste release, instead they will model the potential risk posed by existing vadose zone contamination footprint from past leaks and spills. Information on contamination footprint (i.e., inventory diameter with unit source) is based on spectral gamma data for drywells in the vicinity of Tank C-106.

Two-dimensional flow and transport models along a row of tanks will be used for all vadose zone simulations. The simulations will compose of steady-flow and transient components, where flow fields developed from the steady-flow component will be used to initialize the

transient simulation. Steady-state initial conditions will be developed by simulating from a prescribed unit hydraulic gradient condition to a steady-state condition, dictated by the initial meteoric recharge at the surface, water table elevation, water table gradient, no flux vertical boundaries, variation of hydrologic properties, and location of impermeable tanks.

Figure 2-1. Overall Modeling Approach for Flow and Transport of Residual Wastes, Past Leaks and Retrieval Leaks

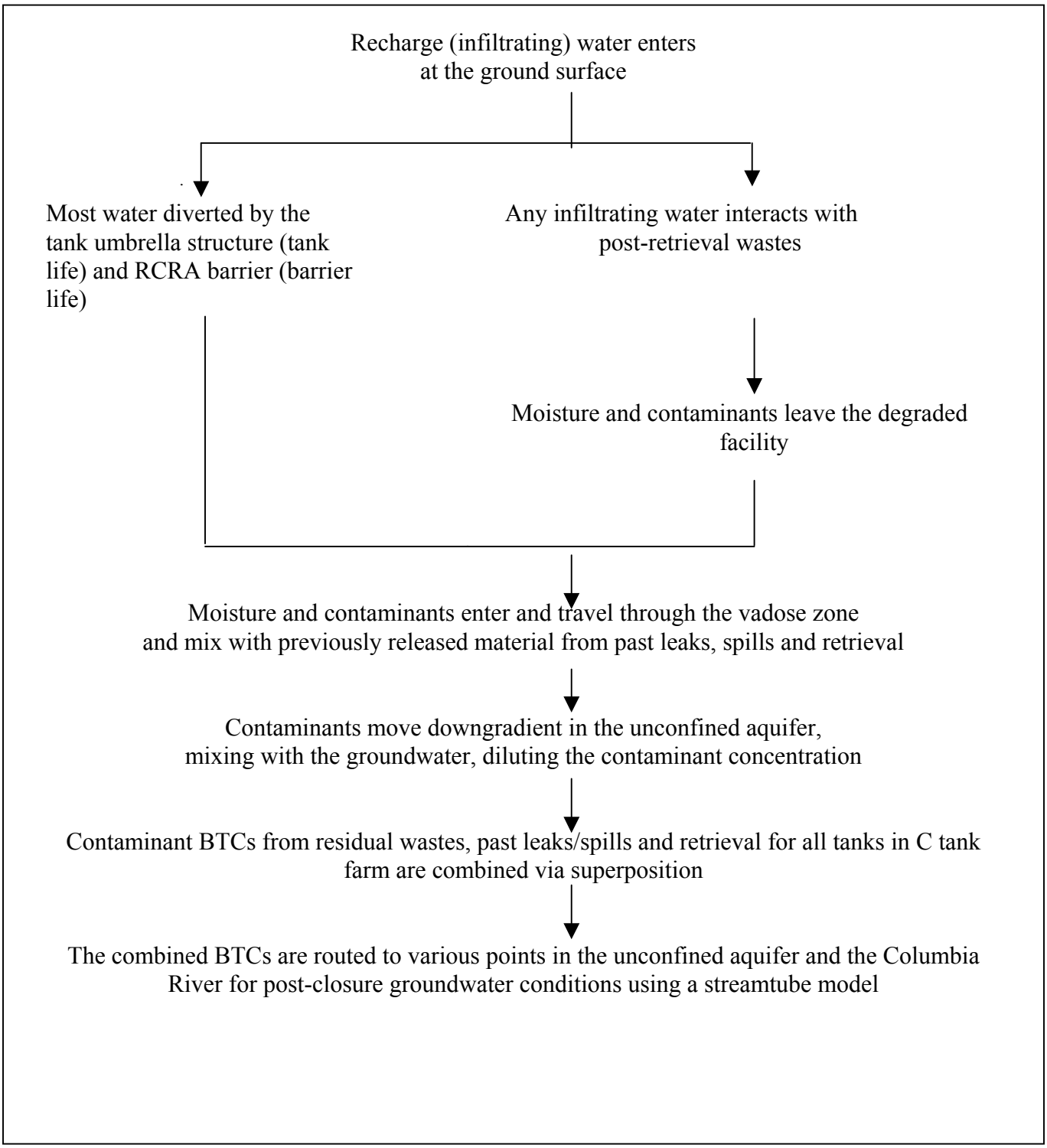

Note that the steady-flow simulation, representing flow conditions for the year 1945 (see Table 4-1), will be used as the initial condition for all subsequent flow and transport simulations. For simulating 1943-44 (Table 4-1) recharge conditions (i.e., the time period prior to construction of C tank farm), the pre-construction material is H1 (gravelly sand) (see Section 3.0). Except for the diffusion-dominated release simulation cases (see Appendix A), the fill material for the tanks, following tank degradation, will be backfill (see Section 3.0). For the diffusion-dominated release simulation cases, grout will be used as the tank fill material (see Section 3.0).

From the starting conditions, transient transport simulations will be conducted for a 10,000-year period (i.e., years 2000 to 12000) that will involve changes in the flow fields in response to current conditions, placement of closure barrier and effects of degraded barrier. The infiltration (recharge) estimates for various times are described in Section 4. All simulations will be run assuming isothermal conditions. The vadose zone will be modeled as an aqueous-gas porous media system where transport through the gas phase is neglected.

Fluid flow within the vadose zone will be described by Richards' equation, whereas the contaminant transport will be described by the conventional advective-dispersive transport equation with an equilibrium linear sorption coefficient (K_d) formulation. A series of mobile to moderately retarded contaminant species (K_d=0, 0.01, 0.03, 0.1, 0.3, 0.6, and 1.0) will be considered for each run.

The geologic strata are assumed continuous but not of constant thickness. A detailed stratigraphic cross-sectional model for the C tank farm is presented in Appendix C; the model includes the effect of dipping strata. The enhanced spreading at the fine-grained/coarse-grained interfaces and the increased downdip movement of the plume along these interfaces will be included in the model. The simulation domain will be extended horizontally to make certain that the prescribed boundary conditions are not violated. The water table is located about 79.84 m (262 ft) below ground surface. Variable grid spacing will be used to model various source terms and features, if any.

No site-specific data are available on soil moisture characteristics for the C tank farm. Data catalogs are, however, available for 200 Area soils. For this work, data on laboratory measurements for moisture retention, particle-size distribution, saturated and unsaturated hydraulic conductivity, and bulk density for individual stratum are based on data for similar soils in 200 East and 200 West Areas (*Modeling Data Package for B-BX-BY Field Investigation Report (FIR)*, Khaleel et al. 2001). For each stratum defined by the stratigraphic cross-sectional model, the small-scale laboratory measurements are upscaled to obtain equivalent horizontal and vertical unsaturated hydraulic conductivities as a function of mean tension, as shown in *Modeling Data Package for S-SX Field Investigation Report (FIR)* (Khaleel et al. 2000). "Upscaled Flow and Transport Properties for Heterogeneous Unsaturated Media" (Khaleel et al. 2002a) and "Effective Hydraulic Conductivity and Macrodispersivity Estimates for Heterogeneous Unsaturated Media" (Khaleel et al. 2002b) show that upscaling of unsaturated hydraulic conductivities (K's) leads to development of macroscopic anisotropies (as a function of mean tension) for each layer (Section 5 and Appendix D). An averaging of van Genuchten

parameters (θ_r, θ_s, α, and n) (*A Closed-Form Solution for Predicting the Conductivity of Unsaturated Soils,* van Genuchten 1980) is used to define a moisture retention curve for each stratum (Section 5 and Appendix D).

In case multiple samples are not available for each stratum, data from other sites in the 200 Areas are used. Attempts are made to use hydraulic properties that were obtained using both laboratory-measured moisture retention and unsaturated hydraulic conductivity. This is primarily to avoid extrapolating the unsaturated conductivities (van Genuchten 1980; "A New Model Predicting the Hydraulic Conductivity of Unsaturated Porous Media" Mualem 1976) to the dry end, based only on saturated conductivity estimate ("Evaluation of van Genuchten-Mualem Relationships to Estimate Unsaturated Conductivity at Low Water Contents," Khaleel et al. 1995). In addition, to reflect field conditions, the laboratory data will be corrected for the presence of any gravel fraction in the sediment samples ("Correcting Laboratory-Measured Moisture Retention Data for Gravels," Khaleel and Relyea 1997). As with flow modeling, each stratum is modeled with different transport parameters (i.e., bulk density, diffusivity, and dispersivity).

An analytical/streamtube approach will be used to model groundwater flow and transport. The analytical solution in *Physical and Chemical Hydrogeology* (Domenico and Schwartz 1990) or any comparable analytical/streamtube model can be used to model saturated transport.

Again, a description of the cases to be modeled is presented later (see Appendix A).

This page is intentionally left blank.

3.0 FACILITY DESCRIPTION AND GEOLOGY

The C-Farm tanks were built during the initial 30-month war-time construction period (1941 to 1944), in the 200 East Area, near the location of the planned C Plant chemical processing facility. The C Tank Farm consists of twelve 100 series tanks and four 200 series tanks (Figure 3-1). The 100 series tanks are 22.9 m (75 ft) in diameter with capacities of 2,010,000 L (530,000 gal). The 200 series tanks are 6.1 m (20 ft) in diameter with capacities of 208,000 L (55,000 gal). Both types of tanks are constructed of reinforced concrete with welded carbon steel liners. These tanks were designed for non-boiling waste with maximum temperatures of 104^0C (220^0F) and a pH of 8-10 (*Tank Characterization Reference Guide*, Simpson et al. 1994).

Figure 3-1. C Tank Farm and Surrounding Facilities.

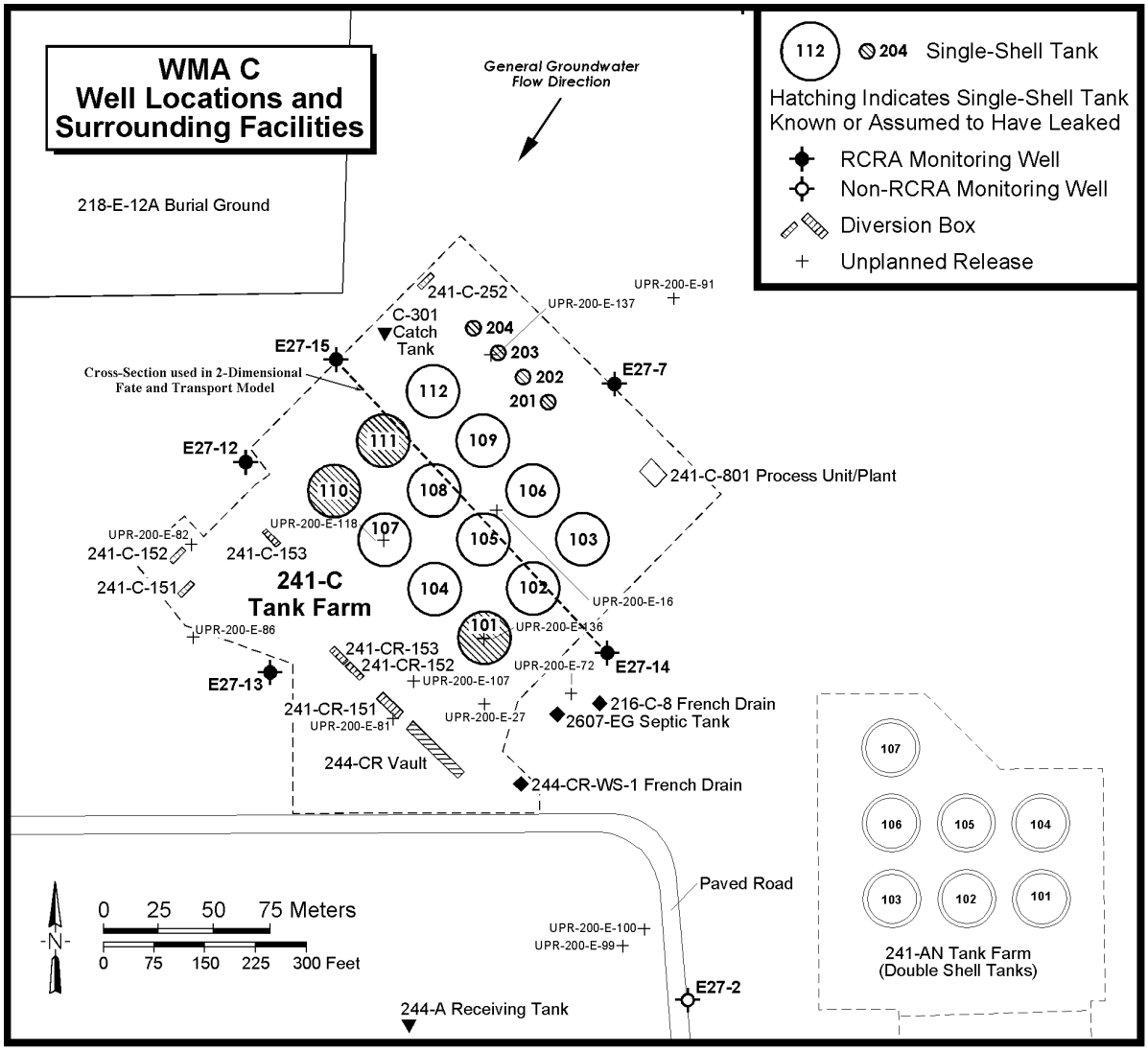

2002/DCL/C/005 (12/30)

Geology. A detailed discussion of C tank farm geology, including the cross-section to be used for modeling, is provided in Appendix C. There are several sedimentary sequences overlying the basalt beneath the C Tank Farm. These are, from top to bottom:

- Backfill (material type 1, sandy gravel),
- Hanford formation - upper gravelly sequence (H1 unit, material type 4, gravelly sand),
- Hanford formation – sand sequence (H2 unit, material type 2, sand),
- Hanford formation - lower gravelly sequence (H3 unit, material type 3, gravelly sand), and
- Undifferentiated Plio-Pleistocene unit gravel (PPlg) and/or Ringold Formation UnitA? (PPlg/(R)? unit, material type 5).

Note that the steady-flow simulation, representing flow conditions for the year 1945 (Table 4-1), will be used as the initial condition for all subsequent flow and transport simulations. For simulating 1943-44 (Table 4-1) recharge conditions (i.e., the period prior to construction of C Tank Farm), H1 (gravelly sand) will be used as the pre-construction material type.

Except for the diffusion-dominated release simulation cases (see Appendix A), the fill material for the tanks, following tank degradation, will be backfill (material type 1, sandy gravel). For the diffusion-dominated release simulation cases, grout will be used as the tank fill material. The van Genuchten parameters for grout are: $\theta_s = 0.5781$, $\theta_r = 0$, $\alpha = 1.08E\text{-}5$ (1/cm), n =1.65, m =1-1/n, $K_s = 1.47E\text{-}8$ cm/s, (*Performance Assessment of Grouted Double-Shell Tank Waste Disposal at Hanford,* Kincaid et al. 1995, v. 1, Table 3.16, p. 3.71).

4.0 RECHARGE RATES, FLOW AND TRANSPORT PARAMETERS

The purpose of this section is to present available data on surface infiltration (recharge). Also presented are effective (upscaled) flow and transport parameters. The effective parameters are based on laboratory measurements for moisture retention, saturated and unsaturated hydraulic conductivity, and bulk density for sediment samples that are similar in particle size distribution to C tank farm sediment samples.

4.1 RECHARGE

C tank farm surfaces are covered with gravel to prevent vegetation growth and provide radiation shielding for site workers. Bare gravel surfaces, however, enhance net infiltration of meteoric water, compared to undisturbed naturally vegetated surfaces. Infiltration is further enhanced in tank farms by the effect of percolating water being diverted by an impermeable, sloping surface of the tank domes. This umbrella effect is created by the 23-m (inside) diameter buried tank domes. Water, shed from the tank domes, flows down the tank walls into underlying sediments. Sediments adjacent to the tanks, while remaining unsaturated, can attain elevated moisture contents. Enhanced infiltration from a gravel-covered tank dome can provide potential for faster transport of contaminants to the water table.

Infiltration (recharge) can vary greatly depending on factors such as climate, vegetation, surface condition, and soil texture. Studies conducted over the last decade at the Hanford Site, such as "Variations in Recharge at the Hanford Site," suggest that recharge rates can vary from less than 0.1 mm/y on a variety of soil and vegetative combinations to greater than 130 mm/y on bare basalt outcrops or bare, gravel-covered waste sites (Gee et al. 1992). Data from experimental sites such as the Field Lysimeter Test Facility (FLTF) and the Prototype Hanford Barrier (PTB), both in the 200 Area, suggest that recharge through gravels can vary from 15 to 70 percent of precipitation, with the lower amount occurring under vegetated conditions (*Hanford Prototype Barrier Status Report FY1996,* Gee et al. 1996; *Estimated Recharge Rates at the Hanford Site,* Fayer and Walters 1995; and *Estimating Recharge Rates for a Groundwater Model Using a GIS,* Fayer et al. 1996). With a long-term annual average precipitation of 160 mm, the higher percentage translates into a recharge rate of about 100 mm/y that was observed on clean gravels that were kept free of vegetation (*Recharge Data Package for the Immobilized Low-Activity Waste 2001 Performance Assessment,* Fayer et al. 1999). Drainage from bare sands is about 55 mm/y (Fayer and Walters 1995) to about 70 mm/y under Hanford climatic conditions (*A Comprehensive Analysis of Contaminant Transport in the Vadose Zone Beneath Tank SX-109,* Ward et al. 1997). There has been no direct measurement of recharge for tank farm gravels, which are known to contain a larger amount of fines than the clean gravels. Thus, it is entirely possible that the tank farms experience a recharge rate that ranges between that observed for bare sand and gravels (Ward et al. 1997). For the purpose of this modeling exercise, a base case infiltration estimate of 100 mm/y will be used prior to closure (Table 4-1).

For simulations involving tank farms with an interim barrier, a recharge rate of 0.5 mm/y will be used. This is based on experimental data, found in "Quest for the Perfect Cap", from a prototype

Hanford barrier that has been designed and built in 200 Area to limit recharge to ≤ 0.5 mm/y (Wing and Gee 1994). This is also supported by the numerical simulation results of *Simulations of Infiltration of Meteoric Water and Contaminant Movement in the Vadose Zone at Single-Shell Tank 241-T-106 at the Hanford Site* (Smoot et al. 1989), which showed that with a relatively impermeable barrier over the tank farm, the drainage to a 2-m backfill depth decreased to less than 0.5 mm/y after 8 years for cases of either a backfill or a clean graveled surface.

The closure barrier for tank farms is assumed to be an enhanced RCRA Subtitle C Barrier with a design life of 500 years; the recharge for such a barrier is estimated to be 0.1 mm/y (Fayer et al. 1999). For the initial assessment calculations, a recharge of 0.5 mm/y will be used. For a degraded closure barrier, recharge rates are expected to return to predevelopment conditions (i.e., shrub-steppe ground cover), with a recharge estimate of 3.5 mm/y. Such an estimate is within the range of values reported in Fayer and Walters (1995).

Table 4-1 summarizes the timeline estimates for barrier emplacement at the C tank farm and the corresponding recharge estimates.

For the tank farm cross-sections, the numerical simulation cases identified in the Appendix A shall commence calculations on January 1, 2000 and continue for 10,000 years. It is assumed that a closure barrier will be in place by 2050. In cases where credit is taken for barrier integrity, it is assumed that a closure barrier will have a design life of 500 years.

For numerical simulations, the initial moisture contents (and the initial matric suctions) for the flow domain will be established by allowing the vadose zone model to equilibrate with an infiltration rate representative of natural infiltration for tank farm location.

Table 4-1. C Tank Farm Infiltration (Recharge) Estimates for Pre-Construction Period, Current Conditions, and Following Emplacement of Closure Barrier.

Condition Simulated	Recharge Estimate (mm/y)	Duration	Comment
Before construction of C tank farm, the construction period being 1943 to 1944	3.5*	Until steady state moisture conditions are achieved for the year 1945	Vadose zone flow simulated at the recharge rate of 3.5 mm/y to develop initial moisture conditions for subsequent simulations
Current conditions	100	1945 to 2050	Recharge is assumed to increase from the pre-construction period estimate of 3.5 mm/y to the current value of 100 mm/y[#]. During this period, the ground cover is gravel with no vegetation. An enhanced RCRA Subtitle C barrier is assumed to be in place by 2050.
Transition to conditions of restricted recharge due to enhanced RCRA Subtitle C barrier	0.5	2050 to 2550	Recharge is assumed to decrease from a current estimate of 100 mm/y to the barrier design value of 0.5 mm/y. The barrier is assumed to function to its design estimate of 500 years[#].
Degraded barrier condition	3.5	2550 to 12000	The barrier is degraded and recharge increases from 0.5 mm/y to 3.5 mm/y until the end of simulation at 12,000 yrs[#].

*Based on 8-yr lysimeter data for graveled surface (Fayer et al.1999)
[#]Appropriate transition periods, as needed, can be used to accommodate the sharp breaks in individual recharge estimates

4.2 FLOW AND TRANSPORT PARAMETERS

This section provides effective (upscaled) values of flow and transport parameters for the vadose zone. Specific flow parameters include moisture retention, saturated and unsaturated hydraulic conductivity. Transport parameters include bulk density, diffusivity, sorption coefficients and macrodispersivity. Details on deriving the effective (upscaled) parameters are addressed in Appendix D.

Table 4-2 lists the composite, fitted van Genuchten-Mualem (van Genuchten 1980; *The RETC Code for Quantifying the Hydraulic Functions of Unsaturated Soils,* van Genuchten et al. 1991) parameters for various strata. Again, note that the material types noted in Table 4-2 (and elsewhere) are identical to those in Figure C-1 (Appendix C). Estimates for the equivalent horizontal and vertical hydraulic conductivities are presented in the Section 4.3.

Table 4-2. Composite van Genuchten-Mualem Parameters for Various Strata.

Strata	Number of samples	θs	θr	α (1/cm)	n	ℓ	Fitted K_s (cm/s)
Backfill (1)	10	0.1380	0.0100	0.0210	1.374	0.5	5.60E-04
Sand H2 (2)	12	0.3819	0.0443	0.0117	1.6162	0.5	9.88E-05
Gravelly Sand H3 (3)	8	0.2688	0.0151	0.0197	1.4194	0.5	5.15E-04
Gravelly Sand H1 (4)	11	0.2126	0.0032	0.0141	1.3730	0.5	2.62E-04
Plio-Pleistocene/ Ringold Sandy Gravel (5)	10	0.1380	0.0100	0.0210	1.374	0.5	5.60E-04

For this initial assessment, a horizontal saturated hydraulic conductivity of 4.8 m/d and a vertical saturated hydraulic conductivity of 0.48 m/d will be used for the unconfined aquifer. Although such estimates are consistent with the saturated media properties for the undifferentiated Plio-Pleistocene/Ringold Gravels, they are much lower than values based on large-scale pumping tests in the 200 East Area. To evaluate sensitivity of results, a horizontal saturated conductivity of 50 m/d (about 10 times larger than 4.8 m/d) will be considered. Such an estimate is consistent with values reported in section 4.3 of RPP-13774.

Presently, all wells in the vicinity of WMA C are completed at the water table and the underlying geology is inferred from wells further away. As part of the RCRA Groundwater Monitoring program, four additional wells are being drilled in the vicinity of WMA C with one well scheduled to penetrate to the base of the aquifer. During the development of this well, a pumping test will be completed and a more representative value of the unconfined aquifer hydraulic conductivity will be obtained.

4.3 STOCHASTIC MODEL FOR MACROSCOPIC ANISOTROPY

As discussed in Appendix D, variable, tension-dependent anisotropy provides a framework for upscaling small-scale measurements to the effective (upscaled) properties for the large-scale vadose zone. A stochastic model, i.e., *Application of Stochastic Methods to Transient Flow and Transport in Heterogeneous Unsaturated Soils* (Polmann 1990) is used to evaluate tension-dependent anisotropy for sediments at the C tank farm; details are in Appendix D. Note that Polmann parameters (Table 4-3) will only be used to assign anisotropy ratios for various strata within the vadose zone.

4.3.1 Macroscopic Anisotropy Parameters

Table 4-3 lists the variable, macroscopic anisotropy parameter estimates for various strata at the waste management area (WMA). Details on derivation of the parameter estimates are in Appendix D.

Table 4-3. Macroscopic Anisotropy Parameters. Based On Polmann (1990) Equations (Appendix D) For Various Strata.

Strata	Number of samples	$<LnK_s>$	$\sigma^2_{LnK_s}$	p	ζ	λ (cm)	A
Backfill (1)	10	-15.76	3.56	-1.1E-4	1.84E-4	30	0.00371
Sandy H2 (2)	12	-14.59	1.50	-7.2E-4	6.55E-4	50	0.00620
Gravelly Sand H3 (3)	8	-15.30	1.83	-5.6E-4	5.16E-4	50	0.00415
Gravelly Sand H1 (4)	11	-14.85	1.94	-2.6E-4	2.50E-4	30	0.00368
Plio-Pleistocene/ Ringold Sandy Gravel (5)	10	-15.76	3.56	-1.1E-4	1.84E-4	30	0.00371

4.4 EFFECTIVE TRANSPORT PARAMETERS

Base case effective transport parameter (bulk density, diffusivity, and dispersivity) estimates are presented in this section. Because of natural variability, the transport parameters are all spatially variable. The purpose is again, similar to the flow parameters, to evaluate the effect of such variability on the large-scale transport process.

4.4.1 Bulk Density and K_d

Both bulk density (ρ_b) and K_d estimates are needed to calculate retardation factors for different species. The effective, large-scale estimate for the product $[\rho_b K_d]$ is the average of the product of small-scale laboratory measurements for bulk density and K_d (*Stochastic Subsurface Hydrology,* Gelhar 1993). Table 4-4 provides the effective, large-scale estimates for Uranium. The average ρ_b, $E[\rho_b]$ (Table 4-4) estimates are based on data in Tables D-1a through D-1d (Appendix D) for various strata. The K_d estimates (Table 4-4) for U are based on *Geochemical Data Package for the Immobilized Low-Activity Waste Performance Assessment* (Kaplan and Serne 1999) data for undisturbed sediments. No other species are included, because the K_d's for Tc-99 and I-129 are estimated to be zero. Calculations (Table 4-4) for $E[\rho_b]$ and $E[\rho_b K_d]$ include correction for the gravel fraction.

Table 4-4. Effective Parameter Estimates, $E[P_bK_d]$, for Uranium for the Product of Bulk Density (g/cm^3) And K_d (cm^3/g).

Strata/Material Type	K_d	$E[\rho_b]$	$E[\rho_bK_d]$
Backfill (1) and Plio-Pleistocene/ Ringold Gravels (5)	0.6	2.13	0.59
Sandy H2 (2)	0.6	1.76	1.04
Gravelly sand H3 (3)	0.6	1.94	1.17
Gravelly sand H1 (4)	0.6	2.07	1.24

4.4.2 Diffusivity

It is assumed that the effective, large-scale diffusion coefficients for all strata at the C tank farm are a function of volumetric moisture content, θ, and can be expressed using the Millington and Quirk (1961) empirical relation:

$$D_e(\theta) = D_0 \frac{\theta^{10/3}}{\theta_s^2} \qquad (1)$$

where $D_e(\theta)$ is the effective diffusion coefficient of an ionic species, and D_0 is the effective diffusion coefficient for the same species in free water. The molecular diffusion coefficient for all species in pore water is assumed to be 2.5×10^{-5} cm^2/sec (Kincaid et al. 1995).

4.4.3 Macrodispersivity

An extended review is provided in Appendix D on the rationale for vadose zone macrodispersivity estimates. Macrodispersivity estimates are needed for both reactive (U) and non-reactive (i.e., Tc-99 and I-129) species.

4.4.3.1 Macrodispersivity Estimates for Non-Reactive Species. Macrodispersivity estimates for non-reactive species (i.e., Tc-99 and I-129) are listed in Table 4-5. Again, details on basis for the estimates are provided in Appendix D.

Table 4-5. Non-Reactive Macrodispersivity Estimates for Various Strata.

Strata	σ^2_{LnK}	Correlation length, λ (cm)	A_L (cm)	A_T (cm)
Backfill (1) and Plio-Pleistocene/ Ringold Sandy Gravel (5)	4.54	30	~150	15
Sandy H2 (2)	4.60	30	~150	15
Gravelly sand H3 (3)	4.95	30	~100	10
Gravelly sand H1 (4)	3.19	30	~100	10

4.4.3.2 Heterogeneous Sorption Enhanced Macrodispersivities for the Reactive Species. As expected, the net effect of sorption is to retard the velocity of the contaminant. Because sorption for specific contaminants may be a function of soil properties, as the soil properties experience spatial variability, the sorption also varies (Gelhar 1993; *Performance Assessment of a Hypothetical Low-Level Waste Facility: Groundwater Flow and Transport Simulation,* Talbott and Gelhar 1994).

Stochastic analysis results for macrodispersivity enhancement for various strata are shown in Table D-6 (Appendix D) for the reactive species (i.e., U). Note that the unsaturated K's were evaluated at -100 cm via the fitted van Genuchten-Mualem relation. The macrodispersivity enhancement ranged from about 1.06 for the H2 sandy sediments to about 1.12 for the H1 gravelly sand sediments (Appendix D).

4.4.3.3 Numerical Considerations. A complicating factor in numerical modeling of contaminant transport in porous media is that both finite-difference and finite-element solutions are affected by "numerical dispersion," which refers to artificial dispersion caused by errors associated with discretization of the flow domain. To minimize such errors, the grid should be designed so that the Peclet number (P_e = discretized distance/dispersivity) is less than or equal to one, although acceptable solutions can be obtained with P_e as high as 10 (*Computational Methods in Subsurface Flow,* Huyakorn and Pinder 1983). With low dispersivities within the vadose zone, the Peclet number criterion results in grid spacings that are not very practical to implement. This is why numerical modelers often resort to higher values of dispersivity. An alternative is to consider use of an "upwinding" option (Huyakorn and Pinder 1983) to control numerical dispersion.

Another consideration is discretization of simulation time so that the Courant number (C_r = pore velocity*time interval/grid spacing) is less than or equal to one. That is, the time step should be selected so that the chosen time interval is less than the value obtained by the ratio of grid spacing to pore velocity. Thus, the time step should be selected so that it is less than the time it takes for the solute to move one grid spacing. Note that, for a three-dimensional problem, the P_e and C_r criteria are applicable to transport in all three directions.

This page is intentionally left blank.

5.0 GROUNDWATER FLOW AND TRANSPORT

5.1 FLOW AND TRANSPORT PARAMETERS

Instead of the Hanford Site-wide groundwater model, an analytical/streamtube approach will be used to model groundwater flow and transport. The analytical solution in Domenico and Schwartz (1990) or any comparable analytical/streamtube model can be used to model saturated transport. Flow and transport information needed for the analytical/streamtube model will be based on VAM3D Site-wide groundwater model, *Hanford Sitewide Groundwater Flow and Transport Model Calibration Report* (Law et al. 1996). Figure 5-1 shows the VAM3D-generated water table map at steady state (post-Hanford conditions) used to generate the streamlines/pathlines, and Figure 5-2 shows a streamline/pathline originating in the vicinity of WMA C.

Information on groundwater velocity distribution is needed for the analytical/streamtube model. Figure 5-1 prescribes the material property numbers for various regions within the flow domain of the Site-wide model. Using Darcy's law, Figure 5-2 combined with Figure 5-3 and Table 5-1, which provides the saturated hydraulic conductivity and porosity for each material type, will be used to perform necessary velocity calculations. Note that a steady-state simulation is being used for the saturated media. In doing so, we can estimate the gradient using the data in Figure 5-1. Note that the water table gradient in the vicinity of WMA C is relatively flat and the aquifer is relatively thin. However, the aquifer resides primarily in the Undifferentiated Plio-Pleistocene unit gravel (PPlg) and/or Ringold Formation UnitA? [PPlg/(R)? unit formation (material type 9 in Table 5-1) with a relatively high saturated conductivity of 0.43×10^5 m/y. The anisotropy ratio (horizontal to vertical) for the saturated media conductivity is a factor of 10 (Table 5-1).

The streamtube analysis will assume that flow directly under WMA C occurs in a southeast direction. *Interim Status Groundwater Monitoring Plan for the Single-Shell Tanks* (Caggiano and Goodwin 1991, see Figure 4 in that document) depicted the generalized flow direction as being due west. Recent results of borescope analysis (June 2002, Figure 5-4) indicate that the flow direction has shifted to the southwest (Figure 5-4). The change in direction is most likely caused by the decline in the hydraulic mound that resulted from the discharges to 216-B-3 Pond (B Pond). As the mound continues to decline, the gradient in the aquifer is expected to continue shifting in a counterclockwise direction until it reestablishes the natural gradient to the southeast that existed before the onset of Hanford discharges altered the regional hydraulics. As contaminants released from the closed tanks are not expected to reach the groundwater for several hundred years, it appears reasonable to assume that the groundwater will have reestablished the natural flow direction by the time they could conceivably do so. A gradient of 4.5×10^{-4} (m/m) will be used, based on pre-Hanford water table map (assumed to be representative of post-closure conditions). Because of the uncertainty with the direction of groundwater flow in the vicinity of the WMA, streamlines for travel northward through the Gable Mountain/Gable Butte Gap also will be considered, in addition to streamlines to the southeast. Other parameters needed for groundwater transport modeling are listed in Table 5-2. The aquifer is relatively thin in the vicinity of WMA C, so for the streamtube model application in the unconfined aquifer, a mixing depth of 5 m will be used.

Figure 5-1. VAM3D-generated steady state hydraulic head (m) distribution for the Hanford Site for post-Hanford conditions (after Lu 1996).

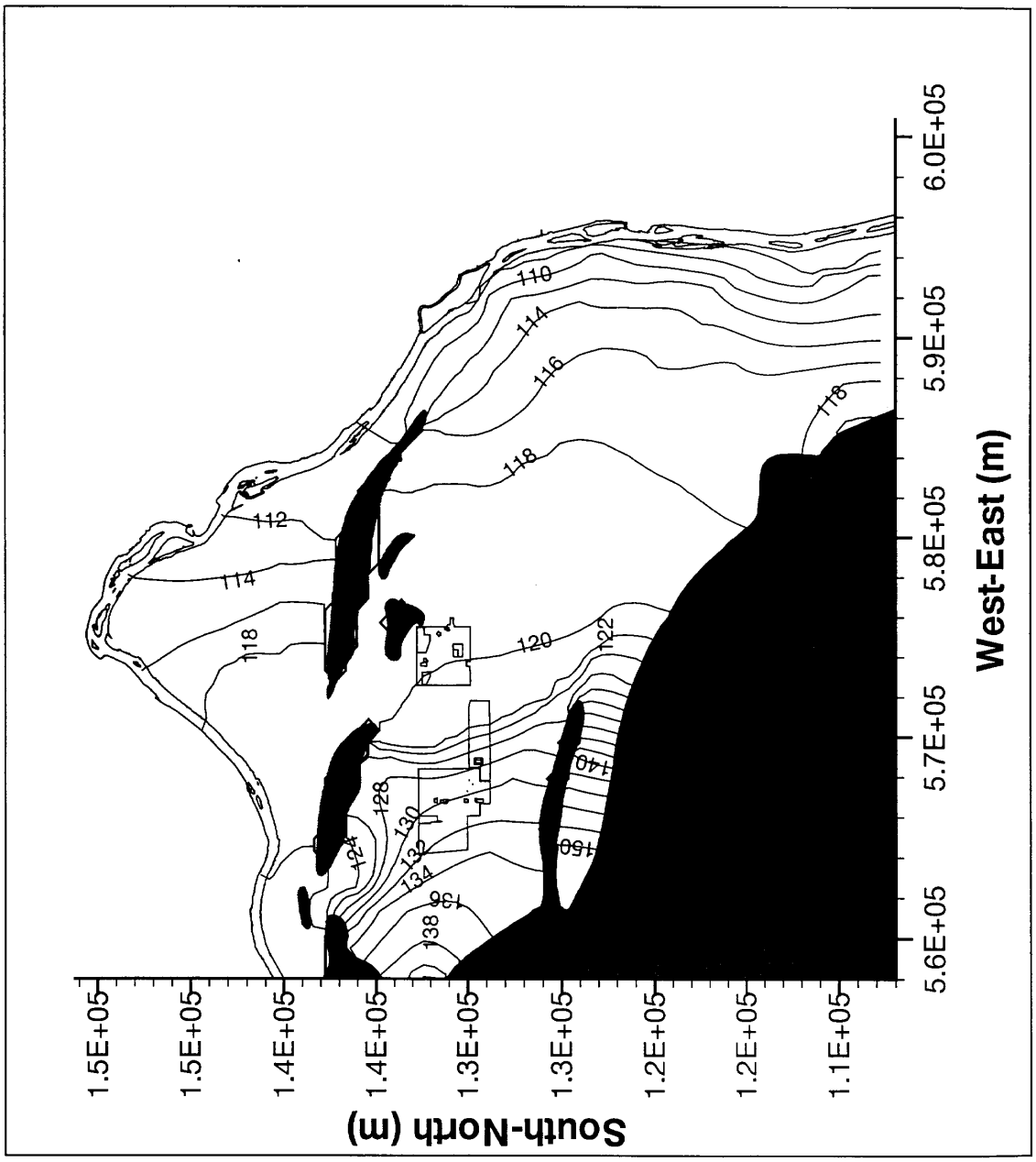

Figure 5-2. VAM3D-Generated Pathline Distribution at Steady State for Post-Hanford Conditions (after Lu 1996).

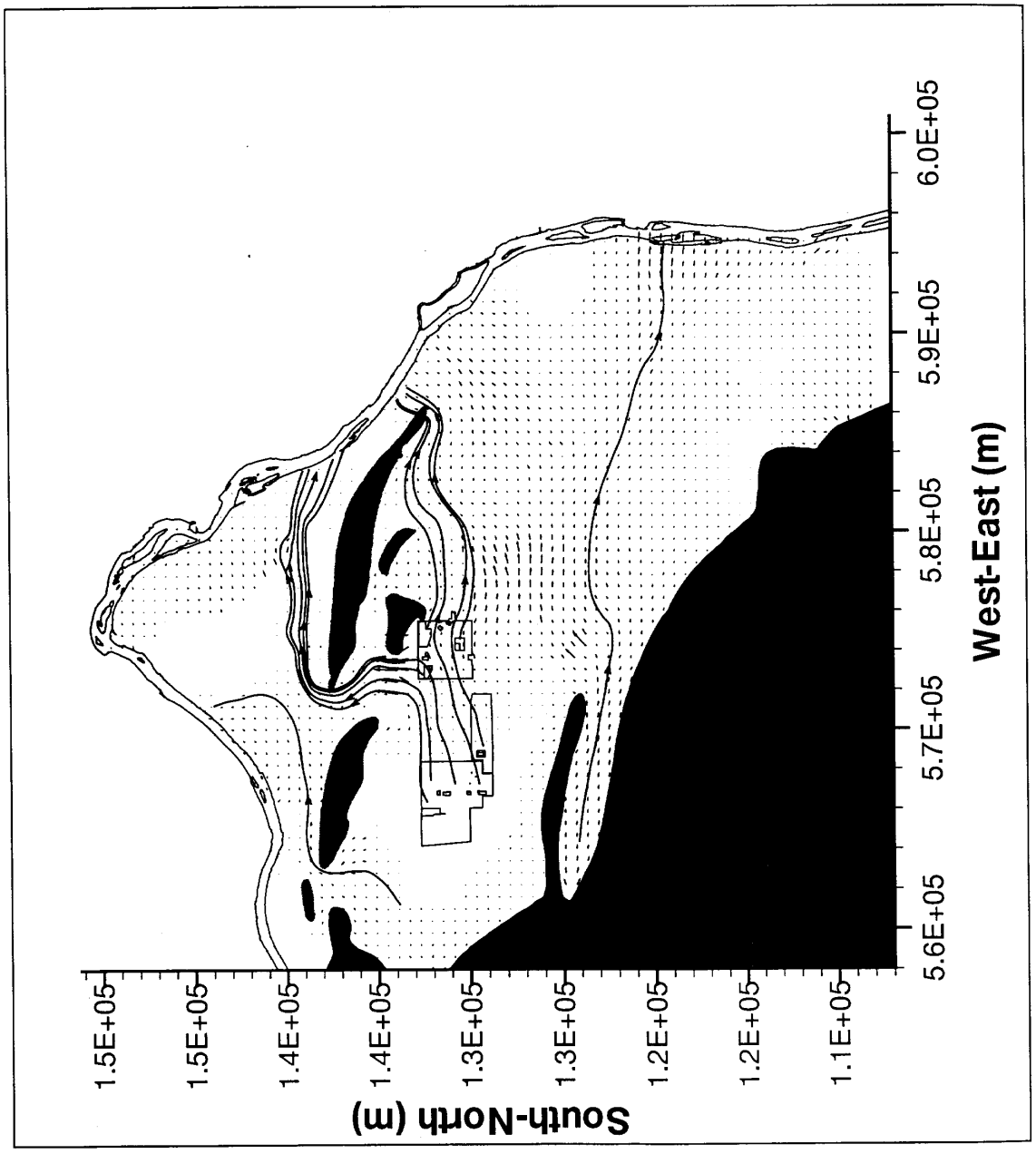

Figure 5-3. Material Property Distribution for the Upper Three Elemental Layers for VAM3D Sitewide Groundwater Model (after Law et al. 1996).

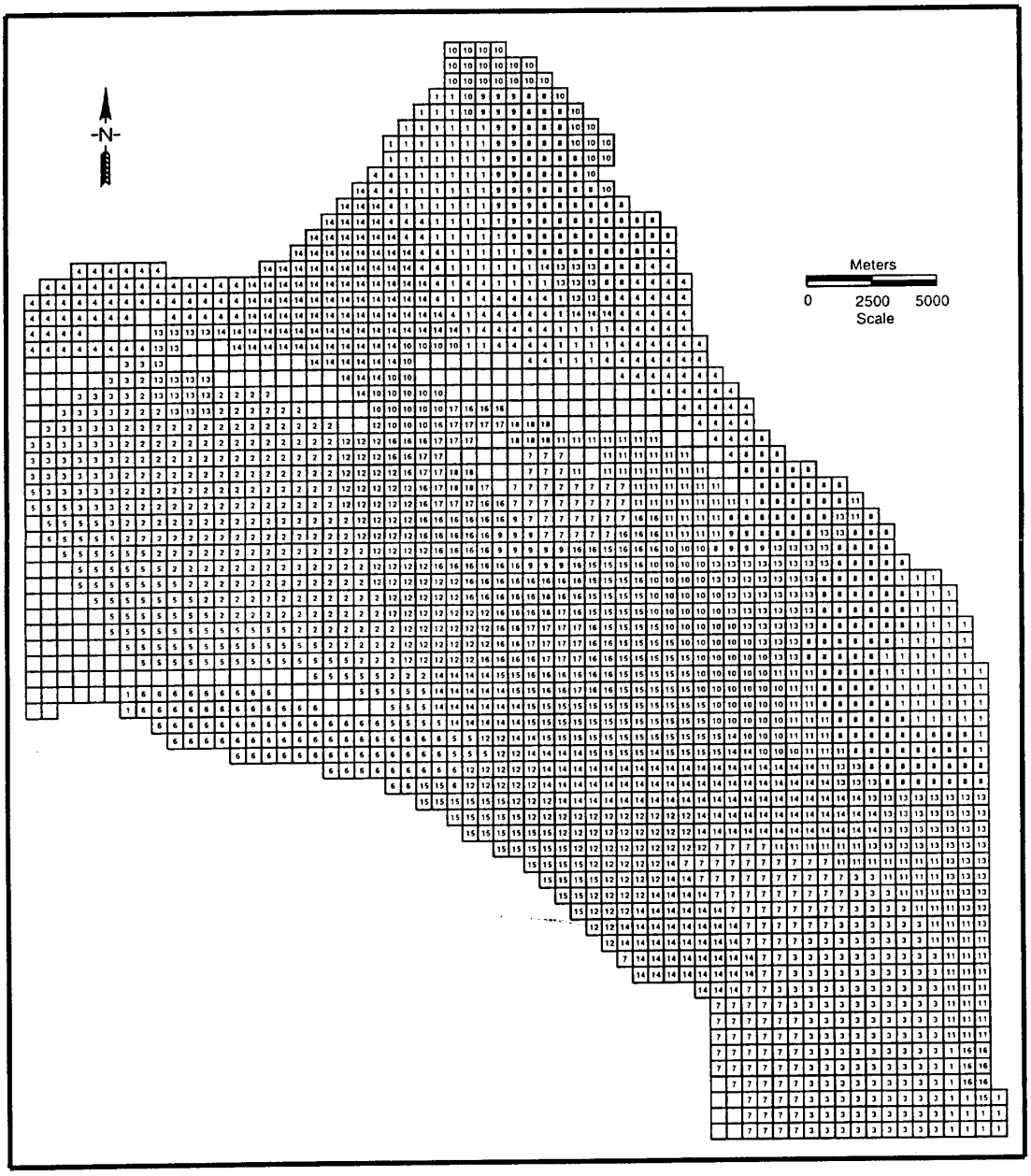

Figure 5-4. Results of Borescope Analysis for Groundwater Flow Direction at WMA C.

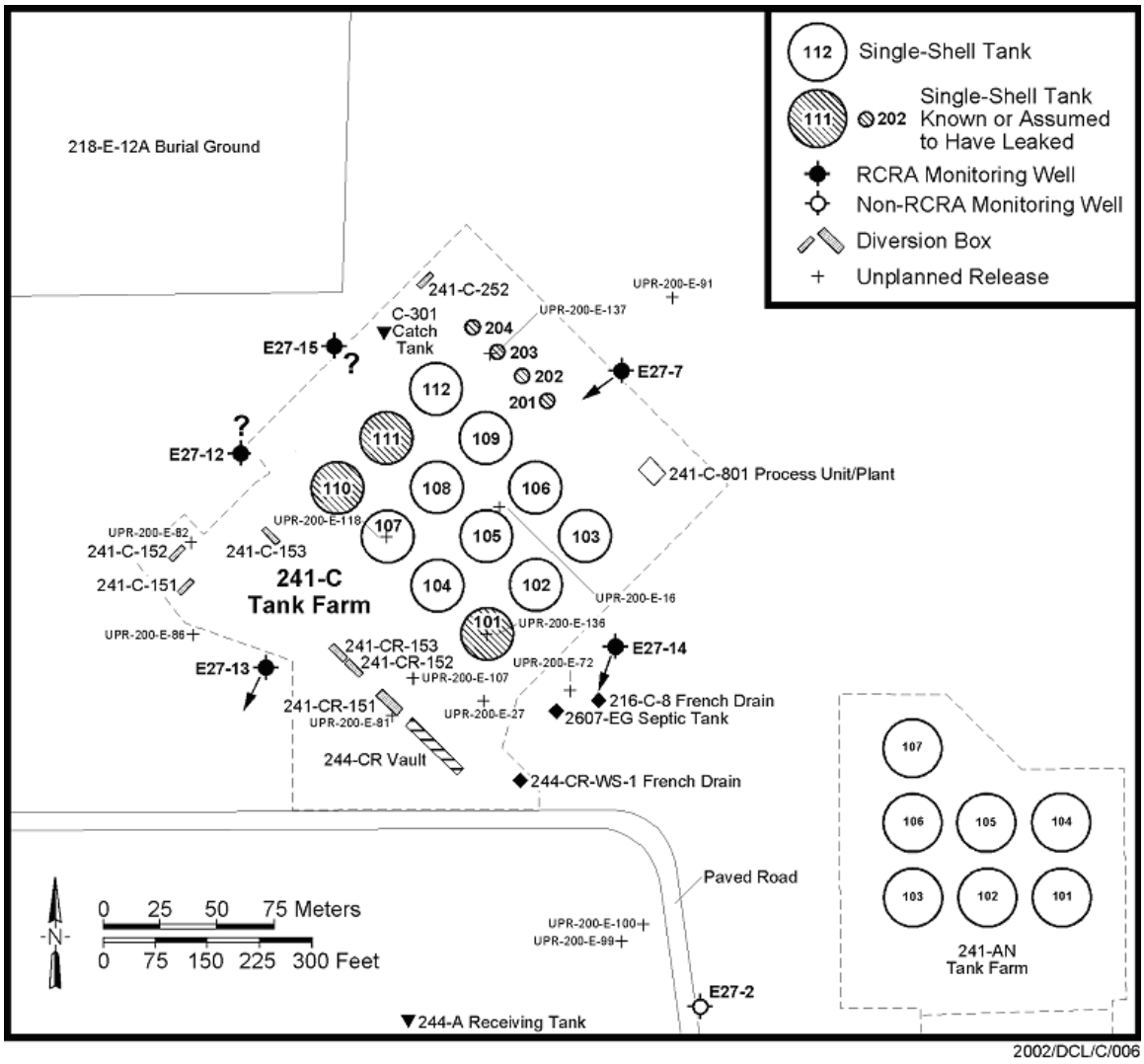

Table 5-1. Hydraulic properties for various material types for Sitewide VAM3D groundwater model (after Law et al. 1996).

Zone	K_{xx} (m/y)	K_{yy} (m/y)	K_{zz} (m/y)	S_s (1/m)	Porosity (Percent)
1	.800E+03	.800E+03	.800E+02	.100E-05	10
2	.190E+04	.190E+04	.190E+03	.100E-05	25
3	.500E+04	.500E+04	.500E+03	.100E-05	10
4	.650E+04	.650E+04	.650E+03	.100E-05	10
5	.140E+05	.140E+05	.140E+04	.100E-05	25
6	.720E+05	.720E+05	.720E+04	.100E-05	25
7	.260E+05	.260E+05	.260E+04	.100E-05	10
8	.300E+05	.300E+05	.300E+04	.100E-05	25
9	.430E+05	.430E+05	.430E+04	.100E-05	25
10	.055E+06	.055E+06	.055E+05	.100E-05	25
11	.770E+05	.770E+05	.770E+04	.100E-05	25
12	.899E+05	.899E+05	.899E+04	.100E-05	25
13	.140E+06	.140E+06	.140E+05	.100E-05	25
14	.300E+06	.300E+06	.300E+05	.100E-05	25
15	.750E+06	.750E+06	.750E+05	.100E-05	25
16	.113E+07	.113E+07	.113E+06	.100E-05	25
17	.183E+07	.183E+07	.183E+06	.100E-05	25
18	.213E+07	.213E+07	.213E+06	.100E-05	25

K_{xx} = Hydraulic conductivity in the North-South direction
K_{yy} = Hydraulic conductivity in the East-West direction
K_{zz} = Hydraulic conductivity in the vertical direction
S_s = Specific storage
m/y = meters per year
1/m = 1 per meter

Table 5-2. Transport parameters for the Site-wide groundwater model.

Parameter	Estimate
Longitudinal macrodispersivity, cm	3050
Lateral macrodispersivity, cm	305
Vertical macrodispersivity, **mm**	10
Diffusion coefficient, cm^2/sec	2.5×10^{-5}
U K_d, cm^3/g	0.6

This page is intentionally left blank.

6.0 REFERENCES

Caggiano, J.A., and S.M. Goodwin, 1991, *Interim Status Groundwater Monitoring Plan for the Single-Shell Tanks*, WHC-SD-EN-AP-012, Westinghouse Hanford Company, Richland, WA.

Domenico, P. A. and F. W. Schwartz, 1990, *Physical and Chemical Hydrogeology,* John Wiley. New York, NY.

Fayer, M. J. and T. B. Walters, 1995, *Estimated Recharge Rates at the Hanford Site,* PNL-10285, Pacific Northwest Laboratory, Richland, WA.

Fayer, M. J., G. W. Gee, M. L. Rockhold, M. D. Freshley, and T. B. Walters, 1996, "Estimating Recharge Rates for a Groundwater Model Using a GIS," *J. Environ. Qual*. Vol. 25, pp. 510-518.

Fayer, M. J., E. M. Murphy, J. L. Downs, F. O. Khan, C. W. Lindenmeier, and B. N. Bjornstad. 1999, *Recharge Data Package for the Immobilized Low-Activity Waste 2001 Performance Assessment,* PNNL-13033, Pacific Northwest National Laboratory, Richland, WA.

Gee, G. W., M. J. Fayer, M. L. Rockhold and M. D. Campbell, 1992, "Variations in Recharge at the Hanford Site," *Northwest Sci*. Vol. 66, pp. 237-250.

Gee, G. W., A. L. Ward, B. G. Gilmore, S. O. Link, G. W. Dennis, and T. K. O'Neil, 1996, *Hanford Prototype Barrier Status Report FY 1996,* PNNL-11367, Pacific Northwest National Laboratory, Richland, WA.

Gelhar, L. W. 1993, *Stochastic Subsurface Hydrology*, Prentice Hall, New York.

Huyakorn, P. S. and G. F. Pinder, 1983, *Computational Methods in Subsurface Flow,* Academic Press, NY.

Kaplan, D.L. and R.J. Serne, 1999, *Geochemical Data Package for the Immobilized Low-Activity Waste Performance Assessment,* PNNL-13037, Pacific Northwest National Laboratory, Richland, WA.

Khaleel, R., J. F. Relyea and J. L. Conca, 1995, "Evaluation of van Genuchten-Mualem relationships to estimate unsaturated conductivity at low water contents," *Water Resources Research,* Vol. 31, pp. 2659-2668.

Khaleel, R. and J. F. Relyea, 1997, "Correcting Laboratory-Measured Moisture Retention Data for Gravels," *Water Resources Research,* Vol. 33, pp. 1875-1878.

Khaleel, R., T. E. Jones, A. J. Knepp, F. M. Mann, D. A. Myers, P. M. Rogers, R. J. Serne, and

M. I. Wood, 2000, *Modeling Data Package for S-SX Field Investigation Report (FIR)*, RPP-6296, Rev. 0, CH2M HILL Hanford Group, Inc., Richland, WA.

Khaleel, R., T. E. Jones, A. J. Knepp, F. M. Mann, D. A. Myers, and M. I. Wood, 2001, *Modeling Data Package for B-BX-BY Field Investigation Report (FIR)*, RPP-9223, Rev. 0, CH2M HILL Hanford Group, Inc., Richland, WA.

Khaleel, R., T.-C. J. Yeh, and Z. Lu, 2002a, "Upscaled Flow and Transport Properties for Heterogeneous Unsaturated Media," *Water Resources Research*, Vol. *38*(5), p. 1053, doi:10.1029/2000WR000072.

Khaleel, R., T.-C. J. Yeh, Z. Lu, 2002b, "Effective Hydraulic Conductivity And Macrodispersivity Estimates for Heterogeneous Unsaturated Media," In *Computational Methods in Water Resources*, Eds. S. M. Hassanizadeh, R. J. Schotting, W. G. Gray, and G. F. Pinder, Proceedings of the XIV International Conference on Computational Methods in Water Resources, Delft, The Netherlands.

Kincaid, C. T., J. W. Shade, G. A. Whyatt, M. G. Piepho, K. Rhoads, J. A. Voogd, J. H. Westsik, Jr., M. D. Freshley, K. A. Blanchard, B. G. Lauzon, 1995, *Performance Assessment of Grouted Double-Shell Tank Waste Disposal at Hanford*, WHC-SD-WM-EE-004, Rev. 1, Westinghouse Hanford Company, Richland, WA.

Kozak, M. W., M. S. Y. Chu, P. A. Mattingly, J. D. Johnson, and J. T. McCord, 1990, *Background Information for the Development of a Low-Level Waste Performance Assessment Methodology*, NUREG/CR-5453 [SAND90-0375], Volume 5, U.S. Nuclear Regulatory Commission, Washington, D.C.

Law, A., S. Panday, C. Denslow, K. Fecht, and A. Knepp, 1996, *Hanford Sitewide Groundwater Flow and Transport Model Calibration Report,* BHI-00608 Rev. 0, Bechtel Hanford, Inc. Richland, WA.

Lu AH. 1996, *Contaminant Transport in the Unconfined Aquifer; Input to the Low Level Tank Waste Interim Performance Assessment,* WHC-SD-WM-RPT-214, Westinghouse Hanford Co., Richland, WA.

Mann, F. M., R. J. Puigh II, S.H. Finfrock, E.J. Freeman, Jr., R. Khaleel, D.H. Bacon, M.P. Bergeron, B.P. McGrail, and S.K. Wurstner, 2001, *Hanford Immobilized Low-Activity Waste Performance Assessment: 2001 Version*, DOE/ORP-2000-24, Rev. 0, U.S. Department of Energy, Richland Operations Office, Richland, WA.

Miller, C. W. 2003. *Data Management Tool Description*, Unpublished report, CH2M HILL Hanford Group, Inc., Richland, WA.

Millington, R. J. and J. P. Quirk. 1961, "Permeability of Porous Solids*," Trans. Faraday Soc,* Vol. 57, pp. 1200-1207.

Mualem, Y., 1976, "A New Model Predicting the Hydraulic Conductivity of Unsaturated Porous Media," *Water Resources Research,* Vol. 12, pp. 513-522.

Polmann, D. J., 1990, *Application of Stochastic Methods to Transient Flow and Transport in Heterogeneous Unsaturated Soils,* Ph.D. Thesis, Massachusetts Institute of Technology, Cambridge, MA.

Simpson, B.C., D.S. DeLorenzo, A.T. DiCenso, D.B. Hiller, K.W. Johnson, J. H. Rutherford, and D. J. Smith, 1994, *Tank Characterization Reference Guide,* WHC-SD-WM-TI-648, Rev. 0., Westinghouse Hanford Company, Richland, WA.

Smoot, J. L., J. E. Szecsody, B. Sagar, G. W. Gee, and C. T. Kincaid, 1989, *Simulations of Infiltration of Meteoric Water and Contaminant Movement in the Vadose Zone at Single-Shell Tank 241-T-106 at the Hanford Site,* WHC-EP-0332, Westinghouse Hanford Company, Richland, WA.

Talbott, M.E. and L.W. Gelhar, 1994, *Performance Assessment of a Hypothetical Low-Level Waste Facility: Groundwater Flow and Transport Simulation,* NUREG/CR-6114 Vol.3, U.S. Nuclear Regulatory Commission, Washington, D.C.

van Genuchten, M. Th, 1980, *A Closed-Form Solution for Predicting the Conductivity of Unsaturated Soils,* Soil Science Society of America Journal, 44:892-898.

van Genuchten, M. Th., F. J. Leij, and S. R. Yates, 1991, *The RETC Code for Quantifying the Hydraulic Functions of Unsaturated Soils*, U.S. E.P.A., EPA/600/2-91/065.

WAC 173-303, ADangerous Waste Regulations@, *Washington State Administrative Code*, Washington State Department of Ecology, as amended.

Ward, A. L., G. W. Gee, and M. D. White, 1997, *A Comprehensive Analysis of Contaminant Transport in the Vadose Zone Beneath Tank SX-109,* PNNL-11463, Pacific Northwest National Laboratory, Richland, WA.

White, M. D., M. Oostrom, M. D. Williams, C. R. Cole, and M. P. Bergeron, 2001, *FY00 Initial Assessments for S-SX Field Investigation Report (FIR): Simulations of Contaminant Migration with Surface Barriers,* PNWD-3111, Battelle, Pacific Northwest Division, Richland, WA.

Williams, M. D., M. Oostrom, and M. D. White, 2001, *Description of Vadose Zone/Groundwater Flow and Transport Numerical Modeling for S Tank Farm Retrieval Performance Evaluation*, Draft report, Pacific Northwest National Laboratory, Richland, WA.

Wing, N. R. and G. W. Gee, 1994, "Quest for the Perfect Cap," *Civil Engineering,* Vol. 64(10), pp. 38-41.

Wood, M. I., R. Khaleel, P. D. Rittmann, A. H. Lu, S. H. Finfrock, R. J. Serne, and K. J. Cantrell, 1995, *Performance Assessment for the Disposal of Low-Level Waste in the 200 West Area Burial Grounds*, WHC-EP-0645, Westinghouse Hanford Company, Richland, WA.

Wood, M. I., R. Khaleel, P. D. Rittmann, A. H. Lu, S. H. Finfrock, T. H. DeLorenzo, and D.Y. Garbrick, 1996, *Performance Assessment for the Disposal of Low-Level Waste in the 200 East Area Burial Grounds*, WHC-SD-WM-TI-730, Westinghouse Hanford Company, Richland, WA.

APPENDIX A

C TANK FARM CLOSURE NUMERIC CALCULATIONS

This page is intentionally left blank.

C TANK FARM CLOSURE NUMERIC CALCULATIONS

The source terms for the risk assessment consist of four separate sources that include (a) past leaks and spills, (b) leakage during retrieval, (c) residual waste leachate from the tanks following closure, and (d) residual waste leachate from the tank ancillary equipment following closure. The past leaks represent tank waste that has leaked into the vadose zone and has been migrating through the vadose zone for a number of years. Retrieval leakage refers to waste leakage to vadose zone that could occur during waste retrieval operations using water-based sluicing. Releases from the residual wastes (both from tank and tank ancillary equipment) in most cases would occur over a long period of time following closure of the tank farm when infiltrating water would enter the tank, dissolve contaminants, and migrate into the vadose zone and to the groundwater. The following items are common to the runs to be performed.

- Except where noted, all calculations are for Tank C-112
- Following Tank C-112 calculations for a unit inventory, contaminant breakthrough curves (BTC's) will be scaled for the actual inventory and a spatial and temporal superposition will be used to obtain BTC's for the entire tank farm based on Tank C-112 results. An equivalency in terms of travel time will be used to extend results based on Tank C-112.
- All calculations will be performed for 10,000 years, i.e., from years 2,000 to 12,000
- A two-dimensional vadose zone flow and transport model will be used
- Unit inventories will be used for all sources
- A series of mobile to moderately retarded contaminant species (K_d=0, 0.01, 0.03, 0.1, 0.3, 0.6, and 1.0) will be considered
- Infiltration rate will be 100 mm/yr from 2000 to 2050, 0.5 mm/yr from 2050 to 2550, and 3.5 mm/yr thereafter
- Isothermal assumption will be used
- Concentrations and fluxes will be reported for the following five surfaces:
    a) One horizontal surface defined by the entire width at the water table.

    b) One vertical surface defined in the aquifer by the tank farm fence line at the bottom right hand edge of the domain.

    c) Three vertical surfaces defined in the aquifer at the centerline distance between tanks (i.e., *approximately* between Tanks C-112 and C-109, between Tanks C-109 and C-106 and between Tanks C-106 and C-103). To establish the actual location of the three vertical surfaces, verification runs (described later) will be performed for different Cases and K_d values.

d) All four of the vertical surfaces will have three sub-surfaces defined at equal 6-m intervals within the saturated aquifer.

Flow and transport simulations and verification tests will be run for the following cases.

- **Case 1: Retrieval leaks, 8000 gallons**. A retrieval leak of 8,000 gallons on the tank corner with start of leakage on 1 January 2000 and continuing for 14 days, with the leak occurring at the bottom east corner of Tank C-112.

- **Case 2: Retrieval leaks, 20000 gallons**. A retrieval leak of 20,000 gallons on the tank corner with start of leakage on 1 January 2000 and continuing for 14 days, with the leak occurring at the bottom east corner of Tank C-112.

- **Case 3: Past leaks**. A past leak with its vadose zone inventory at a depth of 80 ft (based on drywell data) bgs and an inventory diameter of 25 ft (based on drywell data) as of 1 January 2000, with the inventory distributed between Tanks C-112 and C-109.

- **Case 4: Past leaks from ancillary equipment**. A past leak with its vadose zone inventory at a depth of 30 ft bgs (based on drywell data) and an inventory diameter of 25 ft (based on drywell data) as of 1 January 2000, with the inventory distributed between Tanks C-112 and C-109.

- **Case 5: Residual tank waste; release rate R_0**. Residual tank waste source with a release rate R_0 (10^{-3} Ci/yr for 500 yrs and 0.1 Ci/yr for 5 yrs), a release start date of 1 January 2050 (i.e., date tank integrity is lost) and release over the tank bottom.

- **Case 6: Residual tank waste; release rate R_1**. Residual tank waste source with a release rate R_1 (10^{-4} Ci/yr for 500 yrs, 10^{-2} Ci/yr for 95 yrs), a release start date of 1 January 2050 (i.e., date tank integrity is lost) and release over the tank bottom.

- **Case 7: Residual tank waste; release rate R_2**. Residual tank waste source with a release rate R_2 (10^{-5} Ci/yr for 500 yrs, 10^{-3} Ci/yr for 995 yrs), a release start date of 1 January 2050 (i.e., date tank integrity is lost) and release over the tank bottom.

- **Case 8: Residual tank waste; release rate R_3**. Residual tank waste source with a release rate R_3 (10^{-6} Ci/yr for 500 yrs, 10^{-4} Ci/yr for 9,995 yrs), a release start date of 1 January 2050 (i.e., date tank integrity is lost) and release over the tank bottom.

- **Case 9: Residual tank waste; release rate R_4**. Residual tank waste source with a release rate R_4 (0.1 Ci/yr for 10 yrs), a release start date of 1 January 2500 (i.e., date tank integrity is lost) and release over the tank bottom.

- **Case 10: Residual tank waste; advection-dominated release**. Residual tank waste source with advection-dominated release, a release start date of 1 January 2050 (i.e., date tank integrity is lost) and release over the tank bottom.

- **Case 11: Residual tank waste; diffusion-dominated release**. Residual tank waste source with a diffusion-dominated release rate (diffusion coefficient =6 $x10^{-7}$ cm^2/s; Kincaid et al. 1995), a release start date of 1 January 2050 and release over the tank bottom.

- **Case 12: Residual tank waste; diffusion-dominated release**. Residual tank waste source with a diffusion-dominated release rate (diffusion coefficient =5 $x10^{-8}$ cm^2/s; Serne and Wood 1990), a release start date of 1 January 2050 and release over the tank bottom.

- **Case 13: Residual tank waste; solubility-controlled release**. Residual tank waste source with a solubility-dominated release, a release start date of 1 January 2050 (i.e., date tank integrity is lost) and release over the tank bottom.

- **Case 14: Residual ancillary equipment waste**. Residual tank ancillary equipment waste source with inventory located at a depth of 20 ft bgs, a release start date of 1 January 2050, and a diffusion-dominated release (diffusion coefficient =6 $x10^{-7}$ cm^2/s; Kincaid et al. 1995) over an inventory diameter of 25 ft for the grouted residual waste.

- **Verification Tests**. Verification tests for all cases will be performed in which sources will be present at all four tank locations (i.e., the row containing Tanks C-112, C-109, C-106, and C-103) and compared against the case with source for Tank C-112 only. The verification tests will include simulations for K_d = 0 and 0.03.

Groundwater calculations (assuming post-Hanford conditions)

1) For calculations to/near fence line, use an integrated vadose zone and groundwater flow domain

2) Streamtube models will be used to route contaminants from the C tank farm fence line to edge of 200 Area boundary, 200 Area Exclusion boundary and to Columbia River

Summary calculations

1) Unit inventory based BTC's for cases 1 through 12 for Tank C-112 will form the basis for calculations for the entire tank farm.

2) For each tank, for each contaminant, and for each source (residual waste, potential retrieval leaks, past leaks, and tank ancillary equipment), the outputs based on Tank C-112 runs will be scaled.

3) Outputs will be at the C tank farm fence line, 200 Area boundary, 200 Area Exclusion boundary, and the Columbia River (before mixing). The location of the boundaries will be based on the *2002 Initial Assessments for B-BX-BY Field Investigation Report* (FIR): *Numerical Simulations* (Freedman et al. 2002).

REFERENCES

Freedman, V. L., M. D. Williams, C. R. Cole, M. D. White, and M. P. Bergeron, 2002, *2002 Initial Assessments for B-BX-BY Field Investigation Report (FIR): Numerical Simulations*, PNNL-13949, Pacific Northwest National Laboratory, Richland, WA.

Kincaid, C. T., J. W. Shade, G. A. Whyatt, M. G. Piepho, K. Rhoads, J. A. Voogd, J. H. Westsik, Jr., M. D. Freshley, K. A. Blanchard, B. G. Lauzon, 1995, *Performance Assessment of Grouted Double-Shell Tank Waste Disposal at Hanford*, WHC-SD-WM-EE-004, Rev. 1, Westinghouse Hanford Company. Richland, WA.

APPENDIX B

ADVECTION-, DIFFUSION-, AND SOLUBILITY-DOMINATED RELEASE MODELS FOR RESIDUAL WASTES

This page is intentionally left blank.

ADVECTION-, DIFFUSION-, AND SOLUBILITY-DOMINATED RELEASE MODELS FOR RESIDUAL WASTES

As discussed in the main text, the source terms for the risk assessment consist of four separate sources that include (a) past leaks and spills, (b) leakage during retrieval, (c) residual waste leachate from the tanks following closure, and (d) residual waste leachate from the tank ancillary following closure. The past leaks represent tank waste that has leaked into the vadose zone and has been migrating through vadose zone for a number of years. Retrieval leakage to the vadose zone refers to waste leakage that could occur during waste retrieval operations using water-based sluicing.

Releases from the residual wastes (both from tank and tank ancillary equipment) in most cases would occur over a long time period following closure of the tank farm when infiltrating water would enter the tank, dissolve contaminants, and migrate contaminants into the vadose zone and to the groundwater. In addition to the scenarios where the release duration is fixed and are defined in the main text as R_0 through R_4 release scenarios (see Appendix A), three additional models –advection-dominated, diffusion-dominated, and solubility-controlled – will be considered. Unlike the R_0 through R_4 release scenarios, release durations for these three models are not fixed a priori. Detailed descriptions on the three models are presented later. First, the conceptual basis and assumptions for the source term release are presented.

Conceptual Model of Source Term Release. The actual process of contaminant (radionuclides and hazardous chemicals) release for residual wastes from a tank cannot be modeled precisely because of the variability of chemical and physical reactions that occur between the waste material and the infiltrating water. In the real system, contaminants are distributed in a heterogeneous manner within the tank. These contaminants are released into solution at different rates because of the variability in waste material. Finally, variable types and quantities of contaminants are dissolved into the infiltrating water over time, depending on which waste material contacts a particular fluid volume. Therefore, averaging concepts are used in modeling to simplify the mathematical representation of the real system. These concepts must be justified, however, as being a conservative representation of the real system.

The following assumptions are made for the source-term release estimates.

- The release of contaminants from tank residuals is evaluated assuming that the structural integrity of the tanks degrades, allowing recharge (infiltrating) water to enter the tank, and dissolve contaminants from the residuals. The release of contaminants occurs by dissolution of the waste material contaminants into the infiltrating water migrating into and out of tanks through cracks.

- For both stabilized (grouted) and unstabilized (not grouted) residual wastes in tank and tank ancillary equipment, it is assumed that the contaminant inventory will be

available for release into the infiltrating solution via an advection-dominated or a diffusion-dominated or a solubility-controlled release model.

- Unit quantities are assumed for various modeling runs. Because risk estimates are directly proportional to total inventory, the modeling runs with unit quantities can be scaled to calculate risk for any initial inventory.

- Three radionuclides (i.e., Tc-99, I-129 and U-238) are considered for the three release models (i.e., advection-, diffusion-dominated, and solubility-controlled) described below.

- For those stabilized waste materials that are incorporated into a waste form that controls radionuclide release by diffusion (i.e., grout), it is assumed that the diffusion coefficient remains constant over time for the diffusion-dominated release model.

- Contaminant inventories are assumed to be homogeneously distributed among the wastes. For the stabilized, grouted wastes, it is assumed that the contaminants are uniformly distributed in the residual wastes only in the bottom of the tank.

Mathematical Models of Release Mechanisms for the Advection-, Diffusion-, and Solubility-Dominated Models. As indicated earlier, in addition to the R_0 through R_4 release scenarios (Appendix A), the source terms will be estimated by an alternate advection-, diffusion-, or solubility-dominated release model. The mathematical description and conditions under which the different mechanisms occur are provided in the following sections. The area under each release model equals to unit inventory.

Advection-Dominated Release Model. The advection-dominated release model (mixing-cell cascade model) is used to simulate the processes of releases from stabilized (grouted tank or tank ancillary) wastes. For stabilized wastes, the radionuclides exit the facility at a rate determined by the flow of water and the amount of dispersion (mixing) within the tank. The mixing-cell cascade model (Kozak et al. 1990; Wood et al. 1995) is based on the dispersion analysis of chemical reactors and allows the analysis to incorporate the effects of dispersion in the tank in a simplified manner. In this model, the tank inside is considered to be composed of a cascade of N equal-sized, well-stirred cells in series. The total volume of the N cells is equal to the volume of the tank residual waste.

The mixing-cell cascade model for N equal-sized cells is described by the following equation:

$$Q(t) = q\,A\,C_o\,e^{-\alpha\,Nt} \sum_{n=1}^{N} \frac{(\alpha\,Nt)^{n-1}}{(n-1)!}$$

where:
Q = release rate (Ci/yr)
q = vertical Darcy flux (m/yr)
A = horizontal (planar) area of the tank inside
α = q/(θdR)
θ = volumetric moisture content in the residual waste
d = vertical depth of the residual waste material (m)
R = retardation factor in the waste material (assumed R=1).

The initial concentration of contaminant in the interstitial water can be determined from the following equation:

$$C_0 = \frac{m}{\theta VR}$$

where m equals total facility inventory (assumed unity) of the radionuclides in the tank and V equals total volume of the residual waste (i.e., 360 ft^3 or 1% residual following TPA goal). The spatially variable velocities, V, and moisture contents, θ, which are obtained via flow modeling within the tank, will be used to determine C_o. Note that all simulation runs except for Cases 11 and 12 (Appendix A) use backfill as the tank fill material. Cases 11 and 12 use grout as the tank fill material.

The mixing-cell cascade model provides results equivalent to the one-dimensional, convective-dispersion equation with varying values of the dispersion coefficient (Kozak et al. 1990). In the limit, as N approaches infinity, the model represents flow through a system with zero dispersion, whereas for N equal to one, the model represents flow with an infinite dispersion coefficient. A value of N = 10 will be used reflecting moderate dispersion.

Diffusion-Dominated Release Model. The diffusion-dominated release model is used to simulate the release of contaminants from stabilized (e.g., grouted tank or tank ancillary) wastes. In the absence of little or no advection through the waste container, the release can be modeled as a diffusion-limited process. The diffusion from cylindrical containers leads to an expression for flux that contains infinite series (Kozak et al. 1990). The series converges slowly for small diffusion coefficients for short times, and even for relatively long times. As a result, a one-dimensional diffusion solution can be adopted (Crank 1975). The solution, for a semi-infinite medium with the concentration C_0 throughout, initially, and with zero surface concentration, is given by

$$C = C_0 \, erf \frac{x}{2\sqrt{(D_e t)}}$$

where:
erf = standard error function,
D_e = effective diffusion coefficient of the radionuclides in the waste form, and

t = time.

The rate of loss of diffusing substance per unit area from the semi-infinite medium when the surface concentration is zero, is given by:

$$\left(D_e \frac{\partial C}{\partial x}\right)_{x=0} = C_0 \sqrt{\frac{D_e}{\pi t}}$$

The above equation has the form of diffusion mass transfer based on leaching theory. This simplified release model leads to the following form:

$$q = A\, C_0 \sqrt{\frac{D_e}{\pi t}}$$

where:
q = release rate from a single waste cell (Ci/yr),
A = effective surface area of a single cell, and
C_0 = concentration in a cell.

Because the residual waste is likely contained in various cells with differing sizes and shapes, the diffusive release rate, Q, from all residual waste in the tank can be determined by the following equation:

$$Q = C_0 \sqrt{\frac{D_e}{\pi t}} \sum_{i=1}^{n} A_i$$

$$= C_0 A_t \sqrt{\frac{D_e}{\pi t}}$$

where n is the number of cells, A_i is the surface area of individual cells and A_t is total surface area of a tank.

By assuming that the cells are constant, i.e.,

$$I = C_0 \sum_{i=1}^{n} V_i = C_0 V_t$$

where I is the total inventory, V_i is the volume of i-th cell and V_t is the total volume of all cells.

Combining preceding equations, we obtain:

$$Q = I \frac{A_t}{V_t} \sqrt{\frac{D_e}{\pi t}}$$

The ratio A_t/V_t can be replaced by a ratio of a surface area over volume of a tank (only the portion of the tank containing waste will be used to obtain the ratio).

The model calculation is conservative in two aspects. First, the surface area of a tank might not be completely exposed to a moving stream of water. Second, the radionuclides reaching the tank surface area are assumed to be released into the water stream and instantaneously reach the bottom of the tank for release. Two different diffusion coefficient values will be used: 6×10^{-7} cm^2/sec based on Kincaid et al. (1995) and 5×10^{-8} cm^2/sec based on *Hanford Waste-Form Release and Sediment Interaction* (Serne and Wood 1990).

Solubility-Controlled Release Model

Solubility-controlled release models assume that a known solid is present or rapidly forms, and controls the solution concentration in the aqueous phase of the constituents being released. Solubility models are thermodynamic equilibrium models and do not consider kinetics (time required to dissolve or completely precipitate) (Serne and Wood 1990). When identification of the likely controlling solid is difficult, empirical solubility experiments are performed to gather data that can be used to generate an empirical solubility release model. Such empirical models assume a controlling solid and fix the chemistry of all constituents to derive a fixed value for the concentration of specific contaminants. No solubility empirical models presently exist for modeling contaminants from residual tank wastes. However, a solubility-controlled release model (i.e., “cake” model) has often been postulated in previous risk assessments.

The cake model consists of a very simple mathematical formulation containing a recharge rate term, a term for waste solid solubility, and a term for the cross-sectional area of the waste source (i.e., single-shell tank footprint).

The contaminant release mechanism of the cake model is the dissolution of the “structural matrix.” As the matrix dissolves, all the contaminants are assumed to leach congruently at the same rate. When applied to the residual tank wastes, the term "cake" applies to the sludge and hard heel residual in the tanks, which compose the "structural matrix." The release rate for a given contaminant (Tc-99, I-129 and U-238) is given by:

$$dM / dt = -M_o \, A \, Q_w \, C_{wo}^{sol} / M_{wo}$$

where M_{wo} = the original mass of cake (kg). M_{wo} can be derived by the product of tank waste volume (TPA goal of 99% removal) and waste density (1.7 g/cm^3),
M_o = the original quantity of the contaminant in Ci embedded in the cake,
M = M(t) is the current quantity of the contaminant contained in the cake (Ci or kg) at time t,
A = the surface area of the cake exposed to the release mechanism,
C_{wo}^{sol} = the aqueous solubility of the cake simulated as a nitrate salt; the concentration most commonly used is 360 g/L. Based on expected waste characteristics, a value of 72 g/L will be used.
Q_w = the recharge rate in cm/yr, also termed "infiltration rate," and
dM/dt = the rate of loss of contaminant from the cake waste form per unit time t (the rate at which the contaminant enters the vadose zone).

Recharge rates for the cake model are listed in Table l in the main text. Cross-sectional footprint for the cake model consists of the individual tank area.

Tank Ancillary Equipment

Ancillary equipment is defined as structures, piping and equipment outside of the waste tanks but associated with tank farm operations. Evaluating ancillary equipment is an important component of the retrieval and closure strategy evaluation because the equipment potential source term for either worker exposures, if the equipment were to be removed, or long-term risk, if the equipment were left in the tank farm. The ancillary equipment list includes the following categories (DOE-RL 1999):

- Surplus buildings and other surface facilities
- Drywells around C tank farm and RCRA wells, if any
- Riser penetrations
- Leak detection pits
- Cribs and other liquid waste stream disposal sites within the WMA
- Direct buried piping, encased piping, and ventilation elements
- Pump pits, sluice pits, and valve pits associated with individual tanks
- Other facilities such as valve pits, jumper pits, diversion boxes, and structures

Potential sources of contamination include residual waste in the transfer lines, sluicing lines, valve pits, pump pits, and the ventilation system (DOE-RL 1999). For this initial assessment, a unit Curie will be used as tank ancillary inventory. An inventory estimate will, however, be developed for the C tank farm ancillary equipment based on engineering judgment for the volume and characteristics of residual waste that may be present in the ancillary equipment. It is assumed that the residual wastes in ancillary equipment will be stabilized in situ using grout.

References

Crank, J., 1975, *The Mathematics of Diffusion*, Oxford University Press, Oxford, England.

DOE-RL, 1999, *Retrieval Performance Evaluation Methodology for the AX Tank Farm*, DOE/RL-98-72, U.S. Department of Energy, Richland, WA.

Kincaid, C. T., J. W. Shade, G. A. Whyatt, M. G. Piepho, K. Rhoads, J. A. Voogd, J. H. Westsik, Jr., K. A. Blanchard, and B. G. Lauzon, 1995, *Performance Assessment of Grouted Double-Shell Tank Waste Disposal at Hanford*, WHC-SD-WM-EE-004, Revision 1, Westinghouse Hanford Company, Richland, WA.

Kozak, M. W., M. S. Y. Chu, P. A. Mattingly, J. D. Johnson, and J. T. McCord, 1990, *Background Information for the Development of a Low-Level Waste Performance Assessment Methodology*, NUREG/CR-5453 [SAND90-0375], Volume 5, U.S. Nuclear Regulatory Commission, Washington, D.C.

Serne, R. J. and M. I. Wood, 1990, *Hanford Waste-Form Release and Sediment Interaction*, PNL-7297, Pacific Northwest Laboratory, Richland, WA.

Wood, M. I., R. Khaleel, P. D. Rittmann, A. H. Lu, S. H. Finfrock, R. J. Serne, and K. J. Cantrell, 1995, *Performance Assessment for the Disposal of Low-Level Waste in the 200 West Area Burial Grounds*, WHC-EP-0645, Westinghouse Hanford Company, Richland, WA.

This page is intentionally left blank.

APPENDIX C

GEOLOGIC CROSS-SECTION FOR C TANK FARM

This page is intentionally left blank.

GEOLOGIC CROSS-SECTION FOR C TANK FARM

The Waste Management Area (WMA) C lies along the gently sloping, north flank of Cold Creek bar, a large compound flood bar formed during Pleistocene ice-age floods (DOE 1998, Wood et al. 2000) at an elevation of about 650 ft (198 m). The present thickness of the vadose zone measures about 250 ft (76 m) in the vicinity of WMA C (Narbutovskih and Horton 2001; Horton and Narbutovskih 2001). The geohydrologic model of the area in the vicinity of WMA C is based on boreholes located within 1000 ft (300 m) of the WMA and contains an update of previous geologic descriptions given for these areas (Caggiano and Goodwin 1991; Williams et al. 2000; Narbutovskih and Horton 2001; and Horton and Narbutovskih 2001). The geology specific to WMA C was first described by Price and Fecht (1976) followed by Caggiano and Goodwin (1991). Most recently the WMA C geology was summarized by Lindsey (in Narbutovskih et al. 1996) and by Lindsey and Reynolds (in Jones et al. 1998). A total of five stratigraphic units lie within the WMA C. The stratigraphic units are represented on the northwest-southeast cross section (Figure C-1) and are described as follows:

- **Backfill (material type 1, sandy gravel)**: Backfill materials consist of unstructured, poorly sorted mixtures of gravel, sand, and silt removed during tank excavation, and then later used as fill around the tanks. Backfill materials extend to depths of 50 ft within the tank farms. Most or all of the recent deposit eolian sand and silt material found elsewhere across the Hanford Site has been removed and replaced with backfill in the immediate vicinity of the tank-farm WMA's.

- **Hanford formation - upper gravelly sequence (H1 unit, material type 4, gravelly sand)**: Hanford formation H1 unit consists of predominantly loose coarse-grained gravel and sand deposits, with minor beds of sand to silty sand. Coarser beds may contain boulder-sized materials. Only a few weight percent or less $CaCO_3$ has been measured in this unit. The isopach map of the Hanford formation H1 unit suggests the unit thickens along a northwest-southeast trending trough. The maximum thickness (~100 ft [30 m]) of the H1 unit underlies WMA A-AX, but the H1 unit is thinner in the immediate vicinity of the tanks in C tank farm because much of the Hanford formation H1 unit was removed and replaced with backfill during tank-farm construction.

- **Hanford formation – sand sequence (H2 unit, material type 2, sand)**: Hanford formation H2 unit consists of predominantly fine- to coarse-grained sand with lenses of silty sand to slightly gravelly sand. Minor sandy gravel to gravelly sand beds occur sporadically. Consolidation ranges from loose to compact; cementation is very minor or absent, and total $CaCO_3$ content is generally only a few weight percent or less. Silt lenses and thinly interbedded zones of silt and sand are common but not abundant in the Hanford formation H2 unit. These thin (< 1ft [0.3 m]) fine-grained zones generally cannot be correlated among boreholes and are not reflected in the gross gamma-ray logs or moisture data. The Hanford formation sand sequence (H2 unit) underlies the entire area beneath WMA C. The H2 unit thickens to south and west (Figure C-1).

- **Hanford formation - lower gravelly sequence (H3 unit, material type 3, gravelly sand)**: Hanford formation H3 unit consists of predominantly gravelly facies of clast-supported, sandy, pebble to boulder gravel to matrix-supported pebbly sand. The maximum $CaCO_3$ measured is ~2.5 wt%. The exact thickness of the Hanford formation H3 unit beneath WMA C is uncertain.

- **Undifferentiated Plio-Pleistocene unit gravel (PPlg) and/or Ringold Formation UnitA? [PPlg/(R)? unit, material type 5]**: The PPLg/R(?) unit consists of predominantly sandy pebble- to cobble-sized gravel with occasional boulders. As a whole the unit shares characteristics of both coarse-grained facies of the Ringold Formation and the Plio-Pleistocene unit. In some boreholes the unit is described as tight, cemented, and brown colored with oxide coatings (characteristics of the Ringold Formation), whereas borings describe the unit as loose, caving to heaving, losing water, gray colored, and clean/unweathered (more characteristic of the Plio-Pleistocene unit). The total thickness of this unit is <90 ft (27 m), based on a limited number of boreholes where the upper and lower boundaries are represented. The top of PPLg/R(?) unit ranges between 341-407 ft (104-124 m) elevation amsl. The water table lies within this unit.

- **Columbia River Basalt Group**: The Columbia River Basalt Group (CRBG) forms the bedrock base of the unconfined aquifer under WMA C. The top of unit ranges from about 312-344 ft (95-105 m) elevation amsl.

Figure C-1. Northwest-Southeast Cross-Section Through C Tank Farm.

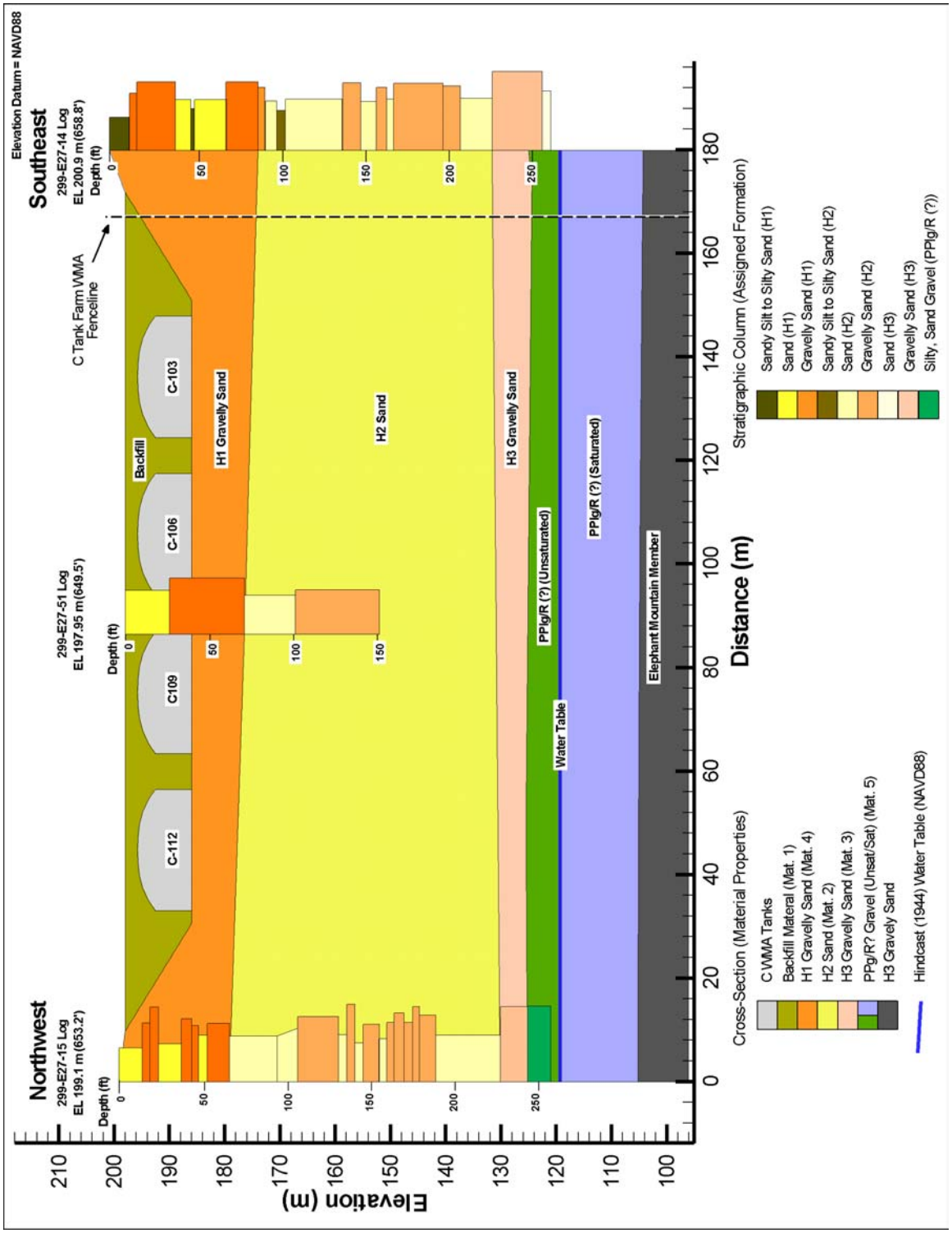

References

Caggiano, J. A., and S. M. Goodwin, 1991, *Interim-Status Groundwater Monitoring Plan for the Single-Shell Tanks*, WHC-SD-EN-AP-012, Rev. 1, Westinghouse Hanford Company, Richland, WA.

DOE, 1998, *Tank Summary Data Report for Tank A-103*, DOE/GJ-HAN-108, U.S. Department of Energy Grand Junction Office, Grand Junction, CO.

Horton, D.G., and S.M. Narbutovskih, 2001, *RCRA Groundwater Monitoring Plan for Single-Shell Tank Waste Management Area C at the Hanford Site*, PNNL-13024, Pacific Northwest National Laboratory, Richland, WA.

Jones, T. E., R. Khaleel, D. A. Myers, J. W. Shade, M. I. Wood, 1998, *A Summary and Evaluation of Hanford Site Subsurface Contamination*, HNF-2603, Rev. 0, Lockheed Martin Hanford, Richland, WA.

Narbutovskih, S. M., and D.G. Horton, 2001, *RCRA Groundwater Monitoring Plan for Single-Shell Tank Waste Management Area A-AX at the Hanford Site*, PNNL-13023, Pacific Northwest National Laboratory, Richland, WA.

Narbutovskih, S. M, D. F. Iwatate, M. D. Sweeney, A. L. Ramirez, W. Daily, R. M. Morey, and L. Christensen, 1996, *Feasibility of CPT-Deployed Vertical Electrode Array in Single-Shell Tank Farms*, WHC-SD-EN-TA-004, Rev. 0, Westinghouse Hanford Company, Richland, WA.

Price, W. H., and K. R. Fecht, 1976, *Geology of the 241-C Tank Farm, ARH-LD-132*, Atlantic Richfield Hanford Company, Richland, WA.

Williams, B. A., B. N. Bjornstad, R. Schalla, and W. D. Webber, 2000, *Revised Hydrostratigraphy for the Suprabasalt Upper Aquifer System, 200 East Area, Hanford Site*, PNNL-12261, Pacific Northwest National Laboratory, Richland, WA.

Wood, M.I., R. Schalla, B.N. Bjornstad, and S.M. Narbutovskih, 2000, *Subsurface Conditions Description of the B-BX-BY Waste Management Area*, HNF-5507, Rev. 0, CH2MHill Hanford Group, Inc, Richland, WA.

APPENDIX D

C TANK FARM VADOSE ZONE FLOW AND TRANSPORT PARAMETER ESTIMATES

CONTENTS

D.1.0 C TANK FARM VADOSE ZONE FLOW AND TRANSPORT PARAMETER ESTIMATES 1
D.1.1 SOIL HYDRAULIC PROPERTIES 1
D.2.0 EFFECTIVE (UPSCALED) FLOW AND TRANSPORT PROPERTIES 4
D.2.1 EFFECTIVE (UPSCALED) FLOW PARAMETERS 4
D.2.1.1 STOCHASTIC UPSCALING 5
D.2.2 EFFECTIVE TRANSPORT PARAMETERS 10
D.2.2.1 BULK DENSITY AND K_d 10
D.2.2.2 DIFFUSIVITY 11
D.2.2.3 DISPERSIVITY 11

LIST OF TABLES

Table D-1. van Genuchten parameters, Fitted Saturated Hydraulic Conductivity, and Measured Bulk Density Data for the Backfill (1) and Plio-Pleistocene/Ringold Sandy Gravel (5) Sediments. 2
Table D-2. van Genuchten Parameters, Fitted Saturated Hydraulic Conductivity, and Measured Bulk Density Data for the Sandy H2 (2) Sequence. 2
Table D-3. van Genuchten Parameters, Fitted Saturated Hydraulic Conductivity, and Measured Bulk Density Data for the Gravelly Sand H3 (3) Sequence. 3
Table D-4. van Genuchten Parameters, Fitted Saturated Hydraulic Conductivity, and Measured Bulk Density Data for the Gravelly Sand H1 (4) Sediments. 3
Table D-5. Composite van Genuchten-Mualem Parameters for Various Strata at the C Tank Farm. 6
Table D-7. Effective Parameter Estimates, $E[\rho_b K_d]$, for U for the Product of Bulk Density (g/cm^3) and K_d (cm^3/g) at C Tank Farm. 11
Table D-8. Non-Reactive Macrodispersivity Estimates for Soils at the C Tank Farm. 17
Table D-9. Macrodispersivity Enhancement Estimates for Various Strata at the C Tank Farm [ρ_b in g/cm^3 and K_d in cm^3/g]. 18

LIST OF FIGURES

Figure D-1. Experimental (Triangles) and Fitted Theoretical (Squares) Variogram for LnKs. 8
Figure D-2. Calculated Macroscopic Anisotropy (Equation D-3) as a Function of Mean Pressure Head for the Backfill (1) and Plio-Pleistocene/Ringold Sandy Gravel (5) Units. 9
Figure D-3. Calculated Macroscopic Anisotropy (Equation D-3) as a Function of Mean Pressure Head for the Sandy H2 (2) Unit. 9
Figure D-4. Calculated Macroscopic Anisotropy (Equation D-3) as a Function of Mean Pressure Head for the Gravelly Sand H3 (3) Sequence. 10

Figure D-5. Calculated Macroscopic Anisotropy (Equation D-3) as a Function of Mean Pressure Head for the Gravelly Sand H1 (4) Unit. 10
Figure D-7. Longitudinal Macrodispersivity in Saturated Media as a Function of Overall Problem Scale with Data Classified by Reliability (after Gelhar et al. 1992). 13
Figure D-8. Longitudinal Macrodispersivity in Unsaturated Media as a Function of Overall Problem Scale (after Gelhar 1993). [Note that the triangles are data from Ward et al. 1998]..... 14
Figure D-9. Uranium LnK versus R for (a) Backfill (1) and Plio-Pleistocene/Ringold Sandy Gravel (5), (b) Sandy H2 (2), (c) Gravelly Sand H3 (3), and (d) Gravelly Sand H1 (4) at the C Tank Farm. 19

This page is intentionally left blank.

D.1.0 C TANK FARM VADOSE ZONE FLOW AND TRANSPORT PARAMETER ESTIMATES

D.1.1 Soil Hydraulic Properties

No site-specific data on soil moisture characteristics are available for vadose zone sediments in the C tank farm. However, as part of other Hanford Site projects, particle-size distribution, saturated hydraulic conductivity, moisture retention and unsaturated conductivity data have been collected in the vicinity of C tank farm. These sites include the ERDF, 241-T-106 tank site, Operable Units 200-UP-1 and 200-UP-2 in 200 West Area. Also available are physical and hydraulic properties data for the sandy gravel sediments in 100 Area along the Columbia River. These samples were used as surrogate to represent the hydraulic properties for the gravel-dominated (>2 mm size fraction) sequence at the C tank farm.

Standard laboratory and Westinghouse Hanford Company quality assurance procedures (WHC 1991) were used to analyze the sediment samples. The moisture retention data for the fine fraction (< 2 mm) and for the drainage cycle of up to -1,000 cm of pressure head were measured using "Tempe" pressure cells; the rest of the drainage data up to -15,000 cm was measured using the pressure plate extraction method (Klute 1986). Saturated hydraulic conductivities for the bulk samples (including gravels) were measured in the laboratory using constant-head permeameter. A variation of the unit gradient method (Klute and Dirksen 1986; Khaleel et al. 1995) was used to measure unsaturated hydraulic conductivities for the bulk samples. The laboratory measured data on < 2 mm size fraction were corrected for the gravel fraction (Gardner 1986; Khaleel and Relyea 1997). No correction was needed for the saturated and unsaturated conductivities, since these were measured on the bulk sample.

It is well recognized that the estimated unsaturated conductivities, based on saturated conductivity and the van Genuchten retention model, can differ by up to several orders of magnitude with measured conductivities at the dry end (e.g., Khaleel et al. 1995). Therefore, a simultaneous fit of both laboratory-measured moisture retention and unsaturated conductivity data was used in this work, and all five unknown parameters θ_r, θ_s, α, n, and K_s, with m=1-1/n (van Genuchten 1980), were fitted to the data via RETC (van Genuchten et al. 1991). The pore size distribution factor, ℓ (Mualem 1976) was kept fixed at 0.5 during the simultaneous fitting. The fitted parameters, based on moisture retention and unsaturated conductivity measurements for various strata are shown in Tables D-1 through D-4. Note that the numbers 1 through 5 in Tables D-1 through D-4 (and elsewhere) represent different strata at the C tank farm.

Table D-1. van Genuchten parameters, Fitted Saturated Hydraulic Conductivity, and Measured Bulk Density Data for the Backfill (1) and Plio-Pleistocene/Ringold Sandy Gravel (5) Sediments.

Sample	Site/ Operable Unit	Borehole Number	Depth (m)	Percent Gravel	θ_s (cm^3/cm^3)	θ_r (cm^3/cm^3)	α (1/cm)	n (-)	Fitted K_s (cm/s)	Bulk Density (g/cm^3)
4-0792	ERDF	699-35-65A	75.4	71	0.100	0.0084	0.03	1.5858	3.42E-04	2.32
4-1012	ERDF	699-35-69A	73.9	55	0.147	0	0.0076	1.5109	4.50E-05	2.19
4-1013	ERDF	699-35-69A	77.9	65	0.139	0.0127	0.0065	1.5656	1.06E-06	2.20
4-1079	ERDF	699-35-61A	90.9	61	0.163	0	0.014	1.3079	1.18E-04	2.06
4-1080	ERDF	699-35-61A	93.5	43	0.178	0	0.0074	1.3819	8.11E-06	2.00
3-0668	241-T-106	299-W10-196	38.9	62	0.175	0	0.0192	1.6124	1.63E-04	2.13
3-0682	241-T-106	299-W10-196	46.1	51	0.224	0	0.0166	1.6577	2.37E-04	2.14
3-0688	241-T-106	299-W10-196	48.5	49	0.199	0	0.0043	1.5321	2.60E-05	2.17
3-0689	241-T-106	299-W10-196	52.2	28	0.236	0	0.0025	1.4747	4.58E-05	1.93
3-0690	241-T-106	299-W10-196	53.7	53	0.1819	0.0177	0.0046	1.541	4.19E-05	2.19

Table D-2. van Genuchten Parameters, Fitted Saturated Hydraulic Conductivity, and Measured Bulk Density Data for the Sandy H2 (2) Sequence.

Sample	Site/ Operable Unit	Borehole Number	Depth (m)	Percent Gravel	θ_s (cm^3/cm^3)	θ_r (cm^3/cm^3)	α (1/cm)	n (-)	Fitted K_s (cm/s)	Bulk Density (g/cm^3)
3-0589	241-T-106	299-W10-196	25.5	1	0.429	0.0268	0.0057	1.7173	4.73E-05	1.86
3-1707	200-UP-2	299-W19-95	9.5	15	0.364	0.0742	0.0082	2.0349	1.55E-05	1.86
3-1712	200-UP-2	299-W19-95	43.1	0	0.290	0.0362	0.0156	2.021	2.05E-04	1.71
3-1713	200-UP-2	299-W19-95	46.3	0	0.5026	0	0.0077	1.6087	2.51E-05	1.72
3-1714	200-UP-2	299-W19-95	50.8	2	0.394	0.1301	0.0061	1.535	1.05E-04	1.68
4-0637	ERDF	699-36-63A	74.9	0	0.378	0	0.0153	1.7309	6.89E-05	1.62
4-0642	ERDF	699-35-69A	25.7	0	0.353	0.0286	0.014	1.4821	6.81E-04	1.98
4-0644	ERDF	699-35-69A	49.8	0	0.394	0.0557	0.0076	1.8353	3.24E-05	1.89
4-0791	ERDF	699-35-65A	63.2	0	0.338	0.0256	0.0226	2.2565	6.81E-04	1.60
4-1076	ERDF	699-35-61A	76.4	0	0.357	0	0.0293	1.7015	1.23E-03	1.74
4-1111	200-UP-1	699-38-68A	56.9	1	0.394	0.0497	0.0093	1.4342	5.80E-05	1.69
4-1112	200-UP-1	699-38-68A	66.0	0	0.4346	0	0.0054	1.4985	2.49E-05	1.73

Table D-3. van Genuchten Parameters, Fitted Saturated Hydraulic Conductivity, and Measured Bulk Density Data for the Gravelly Sand H3 (3) Sequence.

Sample	Site/ Operable Unit	Borehole Number	Depth (m)	Percent Gravel	θ_s (cm^3/cm^3)	θ_r (cm^3/cm^3)	α (1/cm)	n (-)	Fitted K_s (cm/s)	Bulk Density (g/cm^3)
3-0572-2	100-FR-3	199-F5-48	8.1	27	0.179	0	0.0031	1.4306	2.38E-05	2.03
3-0576	100-FR-3	199-F5-43B	5.4	20	0.244	0.0166	0.0167	1.5428	3.96E-04	1.95
3-1707	200-UP-2	299-W19-95	9.5	15	0.364	0.0742	0.0082	2.0349	1.55E-05	1.86
5-0149	218-E-12B	299-E34-1	24.4	16	0.260	0	0.0082	1.4422	1.80E-04	2.07
5-0150	218-E-12B	299-E34-1	24.84	17	0.240	0.0227	0.0295	1.7077	1.47E-03	1.95
5-0151	218-E-12B	299-E34-1	21.49	17	0.275	0	0.0049	1.4621	6.85E-05	1.95
5-0152	218-E-12B	299-E34-1	65.5	26	0.280	0.0252	0.0438	1.3253	2.43E-03	1.85
5-0157	218-E-10	299-E32-4	3.50	13	0.293	0.033	0.0273	2.1675	7.77E-03	1.88

Table D-4. van Genuchten Parameters, Fitted Saturated Hydraulic Conductivity, and Measured Bulk Density Data for the Gravelly Sand H1 (4) Sediments.

Sample	Site/ Operable Unit	Well Number	Depth (m)	Percent Gravel	θ_s (cm^3/cm^3)	θ_r (cm^3/cm^3)	α (1/cm)	n (-)	Fitted K_s (cm/s)	Bulk Density (g/cm^3)
3-0210	241-T-106	299-W10-196	3.1	48	0.186	0.029	0.014	1.7674	1.96E-04	2.11
3-0572-2	100-FR-3	199-F5-48	8.1	27	0.179	0	0.0031	1.4306	2.38E-05	2.03
3-0576	100-FR-3	199-F5-43B	5.4	20	0.244	0.0166	0.0167	1.5428	3.96E-04	1.95
3-0668	241-T-106	299-W10-196	38.9	62	0.175	0	0.0192	1.6124	1.63E-04	2.13
3-0682	241-T-106	299-W10-196	46.1	51	0.224	0	0.0166	1.6577	2.37E-04	2.14
3-0688	241-T-106	299-W10-196	48.5	49	0.199	0	0.0043	1.5321	2.60E-05	2.17
3-0689	241-T-106	299-W10-196	52.2	28	0.236	0	0.0025	1.4747	4.58E-05	1.93
3-0690	241-T-106	299-W10-196	53.7	53	0.1819	0.0177	0.0046	1.541	4.19E-05	2.19
5-0152	218-E-12B	299-E34-1	65.5	26	0.280	0.0252	0.0438	1.3253	2.43E-03	1.85
5-0153	218-E-10	299-E32-4	10.7	47	0.214	0.0092	0.0099	1.3829	1.41E-04	2.08
5-0158	218-E-10	299-E32-4	71.6	44	0.217	0	0.0104	1.3369	4.47E-04	2.15

D.2.0 EFFECTIVE (UPSCALED) FLOW AND TRANSPORT PROPERTIES

Data on hydraulic properties, described in the preceding section, were obtained via laboratory tests on core samples (scales of the order of a few cm). However, numerical models of fluid flow and contaminant transport in the unsaturated zone require specifying hydraulic properties for each discretized grid block (scales of the order of meters). Therefore, the scale of the grid blocks is usually much larger than the scale at which the unsaturated properties were measured. The process of defining large-scale properties for the numerical grid blocks based on small, measurement-scale point measurements is called upscaling.

This section provides effective (upscaled) values of flow and transport parameters for the vadose zone. Specific flow parameters include moisture retention, saturated and unsaturated hydraulic conductivity. Transport parameters include bulk density, diffusivity, sorption coefficients and macrodispersivity.

D.2.1 Effective (Upscaled) Flow Parameters

Any attempt at upscaling is confronted with the issue of spatial variability of hydraulic properties due to small-scale soil heterogeneities. The presence of spatial variability in hydraulic properties of Hanford soils has been well documented (e.g., Khaleel and Freeman 1995). A fundamental issue is then how best to incorporate the effects of natural heterogeneity in modeling. A traditional approach is to use deterministic models and attempt to incorporate the overall heterogeneity of the system such as layering while neglecting the small-scale heterogeneity. The considerable spatial variability of Hanford soils makes complete characterization of the hydraulic properties at the field scale an almost impossible task, as an enormous amount of data is required for proper representation of the actual media heterogeneities.

An alternative approach is to define an equivalent homogeneous medium with average, effective (upscaled) hydraulic properties that are related to the local small-scale heterogeneities and thereby predict the mean flow and transport behavior of the field-scale, larger media. However, to represent a heterogeneous medium by its homogeneous equivalent, we need to estimate the effective hydraulic properties that represent this equivalent homogeneous medium. A straightforward approach would be to use statistical averages (arithmetic or geometric) of the local soil hydraulic properties, but such simple estimates may not always be able to properly describe the complicated nonlinear behavior in heterogeneous soils.

D.2.1.1 Stochastic Upscaling

For saturated media, an averaging of the heterogeneities in geologic media at a smaller scale leads to an effective hydraulic conductivity value, at the larger (macroscopic) scale, with the lateral hydraulic conductivity being much larger than the vertical conductivity (Freeze and Cherry 1979). For unsaturated media, theoretical (e.g., Mualem 1984, Yeh et al. 1985a, b; c, Bear et al. 1987; Mantoglou and Gelhar 1987; Green and Freyberg 1995) and experimental analyses (e.g., Stephens and Heermann 1988; Yeh and Harvey 1990; McCord et al. 1991) of field-scale unsaturated flow indicates that in stratified sediments, the effective hydraulic conductivity tensor is anisotropic with a tension-dependent (or moisture-dependent) degree of anisotropy. The anisotropy ratio of horizontal hydraulic conductivity to vertical hydraulic conductivity increases with decreasing moisture content. Variable, moisture-dependent anisotropy in unsaturated soils is therefore an effective, large-scale (macroscopic) flow property which results from media heterogeneities at a smaller scale, and provide a framework for upscaling laboratory-scale measurements to the effective (upscaled) properties for the large-scale vadose zone.

D.2.1.1.1 Field Observations. Field observations in the 200 Areas do indeed provide evidence of saturation-dependent anisotropy and lateral migration. A test facility comprising an injection well at the center and a radial array of 32 monitoring wells was constructed in 1980 south of PUREX in 200 East Area. The facility was used in late 1980 and early 1981 to conduct an infiltration and multiple tracer (i.e., chloride, nitrate, barium, rubidium, Sr-85 and Cs-134) test, in which 45,000 L of liquid (in 11 increments) were injected at a depth of 4.7 m over a period of 133 days (Sisson and Lu 1984). Three-dimensional water content profiles in layered, coarse sediments were monitored to a depth of 18 m by down-hole neutron probe measurements. The initial water contents were measured at 30-cm increments over the 30- to 1800-cm depths in all 32 observation wells. In situ gamma energy analysis data were collected to determine the distribution of radioactive tracers. The unique three-dimensional nature of the experiment and the measured water content profiles provide evidence of tension-dependent anisotropy. The field data clearly show lateral spreading that occurred during injection. The horizontal wetting patterns dominated the experiment. In fact, numerical modeling results (Sisson and Lu 1984), based on the assumption of a uniform and isotropic model, showed a much deeper penetration of the moisture profile than occurring in the field (Sisson and Lu 1984). The degree of spreading was remarkable considering the apparent uniform lithology at the site.

D.2.1.1.2 Composite Macroscopic Relationships. Both moisture retention and unsaturated conductivity data show spatial variability, although the degree of variation at a given tension is more modest for moisture retention than for hydraulic conductivity. Based on data in Tables D-1 through D-4, composite parameters for the moisture retention relations were determined. The composite van Genuchten parameters for various strata were obtained via RETC (van Genuchten et al. 1991) and a simultaneous fit of both moisture retention and unsaturated conductivity predictions; all four unknown

parameters θ_r, θ_s, α, and n with m=1-1/n (van Genuchten 1980), were fitted to the data. The pore size distribution factor ℓ was kept constant at 0.5 during the simultaneous fitting. The saturated conductivity, K_s, was fitted to the data.

Table D-5 shows the fitted parameters. Equivalent horizontal and vertical hydraulic conductivities are derived using macroscopic anisotropy relations, as described in the next section.

Table D-5. Composite van Genuchten-Mualem Parameters for Various Strata at the C Tank Farm.

Strata	Number of samples	θs	θr	α (1/cm)	n	ℓ	Fitted K_s (cm/s)
Backfill (1)	10	0.1380	0.0100	0.0210	1.374	0.5	5.60E-04
Sand H2 (2)	12	0.3819	0.0443	0.0117	1.6162	0.5	9.88E-05
Gravelly Sand H3 (3)	8	0.2688	0.0151	0.0197	1.4194	0.5	5.15E-04
Gravelly Sand H1 (4)	11	0.2126	0.0032	0.0141	1.3730	0.5	2.62E-04
Plio-Pleistocene/ Ringold Sandy Gravel (5)	10	0.1380	0.0100	0.0210	1.374	0.5	5.60E-04

D.2.1.1.3 Stochastic Model for Macroscopic Anisotropy. As discussed earlier, variable, tension-dependent anisotropy provides a framework for upscaling small-scale measurements to the effective (upscaled) properties for the large-scale vadose zone. A stochastic model is used to evaluate tension-dependent anisotropy for sediments at the C tank farm.

Yeh et al. (1985b) analyzed steady unsaturated flow through heterogeneous porous media using a stochastic model; parameters such as hydraulic conductivity are treated as random variables rather than as deterministic quantities. The Gardner (1958) relationship was used by Yeh et al. to describe unsaturated hydraulic conductivity (K) as a function of saturated hydraulic conductivity (K_s) and tension (ψ), i.e.,

$$K(\psi) = K_s \exp(-\beta\psi) \quad \text{(D-1)}$$

where β is a fitting parameter. Equation (D-1) can be written as

$$\ln K(\psi) = \ln K_s - \beta\psi \quad \text{(D-2)}$$

Equation (D-2) is referred to as the log-linear model, since lnK is linearly related to ψ through the constant slope β. However, such a constant slope is often inadequate in describing lnK(ψ) over ranges of tension of practical interest for field applications. As an alternative, the slope β can be approximated locally by straight lines over a fixed range of tension. The "$\ln K_s$" term in equation (D-2) can then be derived by extrapolating the local slopes back to zero tension.

Using a linear correlation model between the log-conductivity zero-tension intercept and β, Polmann (1990) presents a generalized model that accounts for the cross-correlation of the local soil property (i.e., $\ln K_s$ and β) residual fluctuations. Compared to uncorrelated $\ln K_s$ and β model, partial correlation of the properties is shown to have a significant impact on the magnitude of the effective parameters derived from the stochastic theory. The Polmann (1990) equations for deriving the effective parameters are as follows.

$$
\begin{aligned}
&< LnK >=< LnK_s > -A < \psi > -\sigma^2_{LnKs}\lambda[p - p^2 < \psi > -\zeta^2 < \psi >]/(1 + A\lambda) \\
&\sigma^2_{LnK} = \sigma^2_{LnKs}[(1 - p < \psi >)^2 + \zeta^2 < \psi >^2]/(1 + A\lambda) \\
&K_h^{eq} = \exp[< LnK > +(\sigma^2_{LnK}/2)] \\
&K_v^{eq} = \exp[< LnK > -(\sigma^2_{LnK}/2)]
\end{aligned}
\qquad \text{(D-3)}
$$

where σ^2_{LnK} = variance of log unsaturated conductivity (which depends on mean tension),
<ψ> = mean tension,
σ^2_{LnKs} = variance of $\ln K_s$
<$\ln K_s$>=mean of $\ln K_s$,
p = slope of the β versus $\ln K_s$ regression line,
$\zeta = \sigma_\delta/\sigma_{\ln Ks}$,
σ_δ = standard deviation of the residuals in the β versus $\ln K_s$ regression,
A = mean slope, β, for $\ln K_s$ vs. ψ,
λ = vertical correlation lengths for $\ln K_s$ (assumed to be same as that of β),
K_h^{eq} = equivalent unsaturated horizontal conductivity, and
K_v^{eq} = equivalent unsaturated vertical conductivity.

D.2.1.1.4 Macroscopic Anisotropy Relations. Results of application of equation (D-3) for variable anisotropy are presented below. The data for individual stratum (Tables D-1 through D-4) were used to obtain parameters <lnKs>, $\sigma^2_{LnK\,s}$, p, ζ, and A. The slope and pseduo $\ln K_s$ estimates, discussed in the preceding section, were evaluated for the moisture regime of interest (i.e., tension range of 500 cm to 700 cm for the sandy sequence and 700 cm to 1000 cm for the gravelly sequence). It should be noted, however, that no experimental data are available for unsaturated conductivities in the tension range of interest; β and $\ln K_s$ estimates were based on the fitted van Genuchten-Mualem curves.

An estimate of the correlation length, λ, is needed for anisotropy calculations. Most of the measurements in 200 Areas have been obtained at sampling intervals that are too coarse to yield a reasonable estimate for the correlation length. However, one data set is available that provides saturated conductivity estimates at about 30 cm intervals for a depth of 18 m within the Hanford formation; the site is located about 1/2 mile east of the Immobilized Low-Activity Tank Waste (ILAW) site in 200 East Area. Figure D-1 shows the experimental variogram and the fitted spherical variogram model for saturated conductivities. The fitted spherical variogram suggests a correlation length, λ, of about 50 cm; i.e., the distance at which the variogram drops to [1-(1/e)] times the sill (Figure D-1). The correlation length, λ, for both lnKs and β were assumed to be equal.

The Polmann parameters for various strata are shown in Table D-6. Because of different A, <lnKs>, $\sigma^2_{LnK_S}$, and ζ values, macroscopic anisotropy relations for the sandy and gravelly sediments are quite different. Figures D-2 through D-5 illustrate the macroscopic anisotropy relations for the four sediments, and will be used to assign anisotropy ratios for various strata. In general, the anisotropy for the gravelly soils is much less compared to that for sandy soils. Note that, for gravelly soils, no data were available for a variogram analysis. However, a smaller λ value (30 cm) is used (Table D-6) because of a much higher variance of $\ln K_s$ for the gravelly soils than for the sandy soils.

Figure D-1. Experimental (Triangles) and Fitted Theoretical (Squares) Variogram for LnKs.

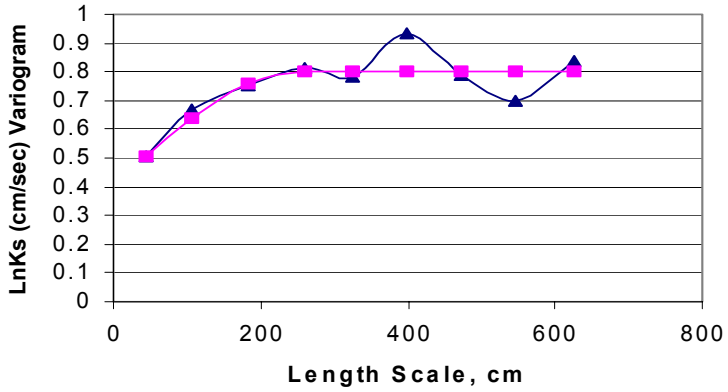

Table D-6. Macroscopic Anisotropy Parameters for Various Strata at the C Tank Farm.

Strata	Number of samples	θs	θr	α (1/cm)	n	ℓ	Fitted K_s (cm/s)
Backfill (1)	10	0.1380	0.0100	0.0210	1.374	0.5	5.60E-04
Sand H2 (2)	12	0.3819	0.0443	0.0117	1.6162	0.5	9.88E-05
Gravelly Sand H3 (3)	8	0.2688	0.0151	0.0197	1.4194	0.5	5.15E-04
Gravelly Sand H1 (4)	11	0.2126	0.0032	0.0141	1.3730	0.5	2.62E-04
Plio-Pleistocene/ Ringold Sandy Gravel (5)	10	0.1380	0.0100	0.0210	1.374	0.5	5.60E-04

Figure D-2. Calculated Macroscopic Anisotropy (Equation D-3) as a Function of Mean Pressure Head for the Backfill (1) and Plio-Pleistocene/Ringold Sandy Gravel (5) Units.

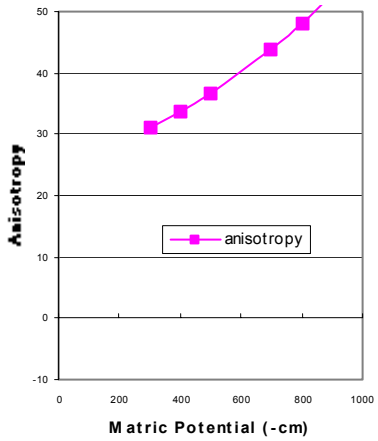

Figure D-3. Calculated Macroscopic Anisotropy (Equation D-3) as a Function of Mean Pressure Head for the Sandy H2 (2) Unit.

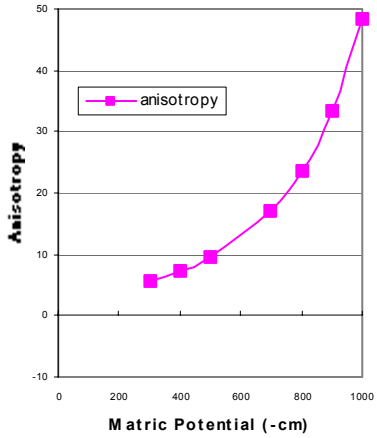

Figure D-4. Calculated Macroscopic Anisotropy (Equation D-3) as a Function of Mean Pressure Head for the Gravelly Sand H3 (3) Sequence.

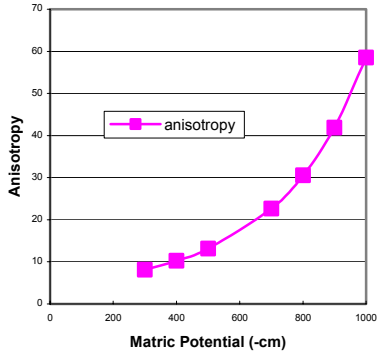

Figure D-5. Calculated Macroscopic Anisotropy (Equation D-3) as a Function of Mean Pressure Head for the Gravelly Sand H1 (4) Unit.

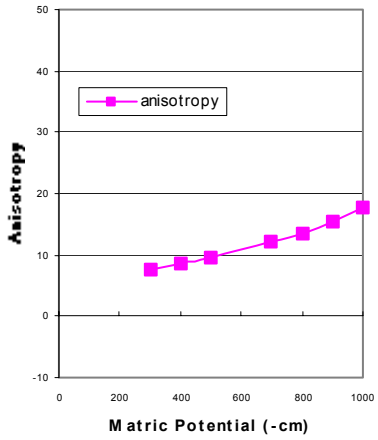

D.2.2 Effective Transport Parameters

Base case effective transport parameter (bulk density, diffusivity, and dispersivity) estimates are presented in this section. Because of natural variability, the transport parameters are all spatially variable. The purpose is again, similar to the flow parameters, to evaluate the effect of such variability on the large-scale transport process.

D.2.2.1 Bulk Density and K_d

Both bulk density (ρ_b) and K_d estimates are needed to calculate retardation factors for different species. The effective, large-scale estimate for the product [$\rho_b K_d$] is the average of the product of small-scale laboratory measurements for bulk density and K_d (Gelhar

1993). Table D-7 provides the effective, large-scale estimates for U. The average ρ_b, $E[\rho_b]$ (Table D-7) estimates are based on data in Tables D-1 through D-4 for various strata. The K_d estimates (Table D-7) for U are based on Kaplan and Serne (1999) data for undisturbed sediments. No other species are included, because the K_d's for Tc-99 and I-129 are estimated to be zero.

Table D-7. Effective Parameter Estimates, $E[\rho_b K_d]$, for U for the Product of Bulk Density (g/cm^3) and K_d (cm^3/g) at C Tank Farm.

Strata/Material Type	K_d	$E[\rho_b]$	$E[\rho_b K_d]$
Backfill (1) and Plio-Pleistocene/ Ringold Gravels (5)	0.6	2.13	0.59
Sandy H2 (2)	0.6	1.76	1.04
Gravelly sand H3 (3)	0.6	1.94	1.17
Gravelly sand H1 (4)	0.6	2.07	1.24

D.2.2.2 Diffusivity

It is assumed that the effective, large-scale diffusion coefficients for all strata at the C tank farm are a function of volumetric moisture content, θ, and can be expressed using the Millington-Quirk (1961) empirical relation:

$$D_e(\theta) = D_0 \frac{\theta^{10/3}}{\theta_s^2} \qquad \text{(D-4)}$$

where $D_e(\theta)$ is the effective diffusion coefficient of an ionic species, and D_0 is the effective diffusion coefficient for the same species in free water. The molecular diffusion coefficient for all species in pore water is assumed to be 2.5×10^{-5} cm^2/sec (Kincaid et al.1995).

D.2.2.3 Dispersivity

An extended review is provided on the rationale of choice for vadose zone dispersivity estimates. Readers who are familiar with the state-of-the-art can proceed directly to Section D.2.2.3.4.

A variety of factors such as the size of the flow domain, the flow regime (saturated versus unsaturated flow), field heterogeneities, and the contaminant species (retarded versus non-retarded) need to be recognized in estimating dispersivities. The objective of this section is to provide appropriate guidance on the choice of vadose zone dispersivity estimates for use in transport modeling.

It should be noted that laboratory data would be of little use in estimating field-scale dispersivities. While well-designed, large-scale tracer experiments would provide useful information, limited field data are available at this time. Therefore, the dispersivity

estimates needed for modeling are essentially based on literature values and the available stochastic equations.

Literature data suggest that much more information is available on dispersion in saturated media than in unsaturated media. Therefore, first the available data on dispersivities in saturated media are summarized (Gelhar et al. 1992). Second, available data on vadose zone dispersivities are presented, including results of small-scale tracer experiments in 200 East Area. Third, the stochastic framework used in obtaining dispersivity estimates is reviewed, and estimates are provided for use in modeling.

D.2.2.3.1 Saturated Media Dispersivities For Field Sites. A critical review of dispersivity observations from 59 different field sites was performed by Gelhar et al. (1992). Extensive tabulations of information were included by Gelhar et al. on aquifer type, hydraulic properties, flow configuration, type of monitoring network, tracer, method of data interpretation, overall scale of observation and longitudinal, horizontal transverse and vertical transverse dispersivities from original sources. The information was then used to classify the dispersivity data into three reliability classes: low, intermediate, and high. Overall, the data indicate a trend of systematic increase of the longitudinal dispersivity with observation scale but the trend is much less apparent when the reliability of data (Figure D-7) is considered. The longitudinal dispersivity ranged from 10^{-1} to 10^{5} m, but the largest scale for high reliability data was only 250 m. When the data are classified according to porous versus fractured media, no significant differences were apparent between these aquifer types. At a given scale, the longitudinal dispersivity values were found to range over 2 to 3 orders of magnitude and the higher reliability data approached the lower portion of this range. The high reliability dispersivity data ranged from a low of about 0.6 m at a scale of 15 m to about 1 m at a scale of 250 m; some data are on the order of 2 to 3.5 m at a scale of 30 m (Figure D-7). It is not appropriate to represent the longitudinal dispersivity data by a single universal line. The variations in dispersivity reflect the influence of differing degrees of aquifer heterogeneity at different sites. The data on transverse dispersivities are more limited but clearly indicate that vertical transverse dispersivities are typically an order of magnitude smaller than horizontal transverse dispersivities (Gelhar et al. 1992). Reanalysis of data from several of the field sites showed that improved interpretations most often lead to smaller dispersivities (Gelhar et al. 1992). Overall, Gelhar et al. concluded that longitudinal dispersivities in the lower part of the indicated range are more likely to be realistic for field situations. This suggests that, for conservative species, a longitudinal dispersivity of the order of a meter is a reasonable estimate for saturated media domains that are a couple of hundred meters in scale. Note that the estimates are for saturated media and conservative species. As discussed later, dispersivity estimates are enhanced due to heterogeneous sorption in both saturated and unsaturated media.

Figure D-7. Longitudinal Macrodispersivity in Saturated Media as a Function of Overall Problem Scale with Data Classified by Reliability (after Gelhar et al.1992)

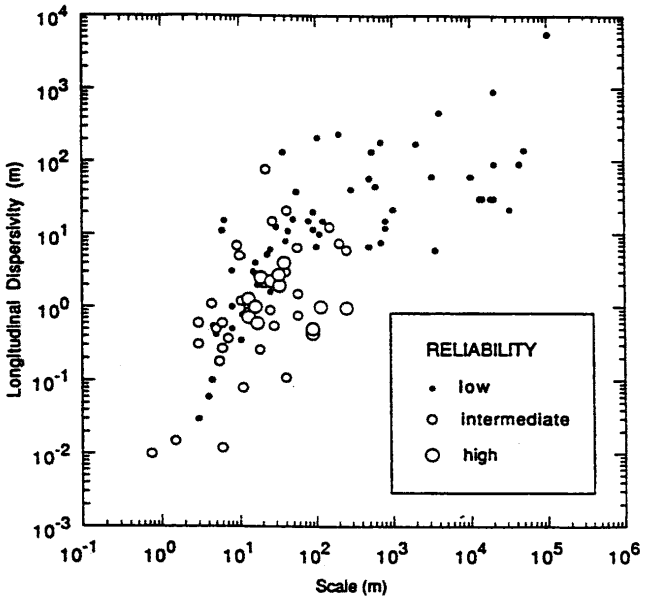

D.2.2.3.2 Vadose Zone Dispersivities. As discussed earlier, for tank farm with a surface barrier, the vadose zone water contents beneath the facility are expected to approach the natural moisture regime for arid soils. Although exceptional precipitation events may cause transient high water contents near the soil surface, the source of the infiltration is not likely to be sustained at great depths within the vadose zone.

This inference is supported by the results of artificial tracer experiments on much shorter time scales. For example, two massively instrumented solute transport experiments were performed in desert soils near Las Cruces, New Mexico (Wierenga et al. 1991; Hills et al. 1991). Drip emitters were used to irrigate a plot adjoining a deep trench in a heterogeneous soil possessing well in excess of one order of magnitude standard deviation in saturated hydraulic conductivity. Monitoring of the trench face showed a spatially uniform progression of the wetting front and did not reveal indications of preferential flow (Wierenga et al. 1991). Hills et al. (1991) found that a dispersivity of 5 cm provided reasonably realistic simulations of ^{3}H and Br tracer distributions.

Figure D-8. Longitudinal Macrodispersivity in Unsaturated Media as a Function of Overall Problem scale (after Gelhar 1993). [Note that the triangles are data from Ward et al. 1998]

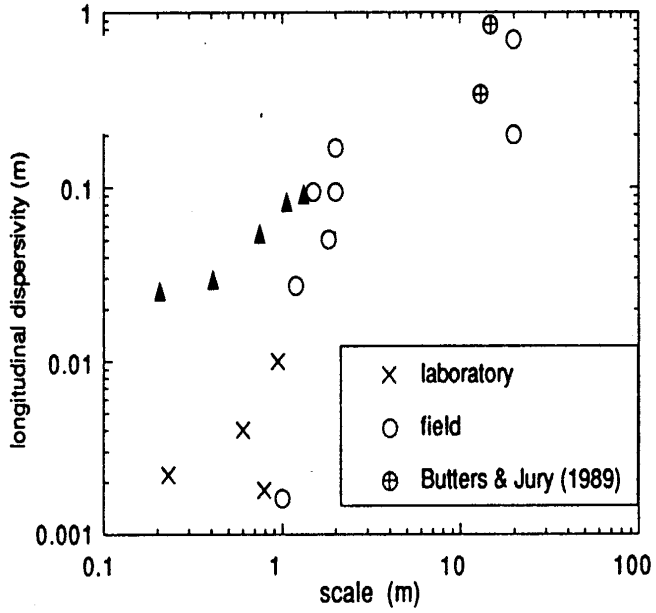

For unsaturated flow, long-term environmental tracer studies at several arid southwestern sites indicate dispersivities of less than 10 cm. Phillips et al. (1988) assessed the degree of mixing in desert soils using the conventional advection-dispersion modeling, yielding a dispersion coefficient of 50 cm^2/yr. This compares with the calculated effective diffusion coefficient of 25 cm^2/yr. A similar study by Scanlon (1992), at another southwestern arid site, obtained a dispersion coefficient of about 14 cm^2/yr. These, then, lead to effective dispersivities of about 7 and 4 cm, at the two arid sites, and Peclet numbers (displacement divided by dispersivity) of 23 and 17.

Ward et al. (1998)[1] obtained dispersivity estimates via field measurements at a location in 200 East Area, using KCl as a tracer. Analysis of the data provided dispersivities that ranged from 1.3 to 7.8 cm for travel distances ranging from 25 to 125 cm. Dispersivity increased with depth to about 0.75 m, after which it essentially became constant. Although these estimates are for the Hanford formation, the transport distance within the vadose zone is indeed of limited extent. Nevertheless, results based on the limited data are consistent with the concept of a scale-dependent dispersivity. Thus, although no data exist on large-scale dispersivities, it is expected that they will be larger than those based on the small-scale tracer experiment of Ward et al. (1998).

[1] Ward, A. L., R. E. Clayton, and J. S. Ritter, 1998, *Determination of in situ hydraulic parameters of the upper Hanford formation.* Letter Report to Fluor Daniel Northwest, Inc., from Pacific Northwest National Laboratory, Richland, WA.

Based on a survey of literature, Gelhar (1993) presented, as shown in Figure D-8, the longitudinal vadose zone dispersivities as a function of the scale of the experiment. The figure shows a lack of data for scales larger than 2 m. Nevertheless, similar to saturated flow, Figure D-8 show an increase of dispersivity with an increase in scale. Also, shown in Figure D-8 are results from the Ward et al. experiment; their data are in close agreement with others.

D.2.2.3.3 Stochastic Models and Macrodispersivities for Large-Scale Media. Field-scale dispersivities are referred to as macrodispersivities. The heterogeneities that exist at various length scales result in a scale dependence of macrodispersivities. Stochastic models have been developed which relate the macrodispersive spreading to the spatial variability of saturated hydraulic conductivity field in a saturated porous media (e.g., Gelhar and Axness 1983; Dagan 1984). The Gelhar and Axness (1983) model provides the asymptotic estimates of macrodispersivity, while the Dagan (1984) model describes the preasymptotic estimates of macrodispersivities for the near-source, early-time period. The Dagan (1984) model predicts that under steady state flow with a uniform mean hydraulic gradient, the ensemble longitudinal macrodispersivity increases with time and displacement distance as the solute first enters the flow domain. A constant, asymptotic value (i.e., Fickian behavior) is eventually reached after the solute travels a few tens of correlation scales of the hydraulic conductivity field.

For prediction of contaminant transport during early time or for short travel distances, simulating effects of scale-dependence on macrodispersion is a consideration. The dispersivities increase with time (or equivalently with distance) until they tend to converge on their unique asymptotic (large time) values. The second-moment evolution curve or the time-dependent, preasymptotic macrodispersivities are of particular interest, since it can take a long time (e.g., years or decades) for the asymptotic Fickian approximation to take hold. However, the early time scale dependence are of little consequence in simulations involving long times or large mean travel distances such as those for C modeling. For these predictions over large travel distances or large times, the use of a constant (asymptotic) dispersivity is considered to be adequate. An estimate of the maximum or asymptotic value of macrodispersivity for saturated media can be based on Gelhar and Axness' (1983) stochastic solution:

$$A_L = \sigma^2_{LnKs} \lambda \qquad \text{(D-5)}$$

where λ is the vertical correlation scale (i.e., average distance over which conductivities are correlated) for log saturated hydraulic conductivity.

In addition to the size of flow domain and vadose zone soil heterogeneities, dispersivities are expected to be a function of soil moisture content (or matric potential). Macrodispersivities are expected to increase with a decrease in saturation (e.g., Polmann 1990; Gelhar et al. 1994). Russo (1993) suggests that vadose zone macrodispersivities can be defined in a manner similar to saturated media estimates. This is based on his finding that the product of the variance and the correlation scale of log conductivity for

both saturated and unsaturated media are of similar magnitude. In other words, an increase in the variance of log conductivity (and, concurrently, in the velocity variance) as moisture content decreases is compensated in part by a decrease in the correlation scale of log conductivity (and, concurrently, in the correlation scale of the longitudinal component of the velocity). Such an approximation (a) assumes use of Gardner's (1958) equation to describe unsaturated conductivity as a function of matric potential, and (b) holds as long as the correlation scale of β in Gardner's equation is relatively small compared with that of log saturated conductivity.

D.2.2.3.4 Macrodispersivity Estimates For Non-Reactive Species.

The Gelhar and Axness equation can be used to estimate asymptotic values of macrodispersivity. However, to account for the effects of unsaturated flow, a modified version is used for C modeling:

$$A_L(<\psi>) = \sigma^2_{LnK}\lambda \qquad \text{(D-6)}$$

where the longitudinal macrodispersivity depends on the mean tension $<\psi>$. To apply equation (D-6), an estimate of the vertical correlation scale for unsaturated conductivity is needed. As discussed earlier, a correlation length of the order of about 50 cm was used for sediments at the C tank farm. However, compared to the saturated K's, an increase in the variance of log conductivity is expected to be compensated in part by a decrease in the correlation scale of log unsaturated conductivity. A correlation length of 30 cm is assumed for log unsaturated conductivity for all five strata. Table D-9 provides the log unsaturated conductivity variances and the estimated longitudinal (A_L) and transverse (A_T) macrodispersivities for various strata. The transverse dispersivities are estimated as $1/10^{th}$ of the longitudinal values (Gelhar et al. 1992). Gelhar (1993) presented results of stochastic analysis of macrodispersion in unsaturated media by Mantoglou and Gelhar (1985). The large-scale macrodispersivity estimates in Table D-9 are of similar magnitude to those reported in Gelhar (1993) for Panoche and Maddock soil types.

D.2.2.3.5 Heterogeneous Sorption Enhanced Macrodispersivities

As expected, the net effect of sorption is to retard the velocity of the contaminant. Because sorption for specific contaminants may be a function of soil properties, as the soil properties experience spatial variability, the sorption also varies (Gelhar 1993; Talbott and Gelhar 1994). The variation directly affects the velocity of the contaminant, which, in turn, enhances the spreading of the plume. The enhanced spreading is defined by a larger reactive longitudinal macrodispersivity, different from the non-reactive

Table D-8. Non-Reactive Macrodispersivity Estimates for Soils at the C Tank Farm.

Strata	σ^2_{LnK}	Correlation length, λ (cm)	A_L (cm)	A_T (cm)
Backfill (1) and Plio-Pleistocene/ Ringold Sandy Gravel (5)	4.54	30	~150	15
Sandy H2 (2)	4.60	30	~150	15
Gravelly sand H3 (3)	4.95	30	~100	10
Gravelly sand H1 (4)	3.19	30	~100	10

longitudinal macrodispersivity, as discussed in the preceding section. The increased plume spreading due to heterogeneous sorption (over and above the result for no sorption) is defined as the macrodispersivity enhancement. Stochastic theory and field data on contaminant plumes suggest that the effect of macrodispersivity enhancement only occurs in the longitudinal direction. The transverse macrodispersivity is unaffected by sorption variability (Garabedian et al. 1991).

The only radionuclide considered for sorption enhancement is uranium; other nuclides have zero K_d. Ideally, to evaluate sorption enhancement, unsaturated hydraulic conductivity measurements and K_d for each species are needed on the same soil samples. However, this was not possible for the samples utilized in this work.

Stochastic theory developed by Gelhar (1993) was evaluated to determine the importance of varying longitudinal macrodispersivity by contaminant species on the basis of sorption heterogeneity and correlation with hydraulic conductivity. An enhancement of macrodispersivity can have significant effects on the expected contaminant movement predictions for numerical models.

In order to understand clearly the importance of heterogeneous, spatially variable sorption, a number of parameters were defined. The variable K_d may be prescribed by a mean (K_d) and a standard deviation (σ_{Kd}). Further, a retardation factor, R, was related to K_d by the following:

$$R = 1 + \frac{\rho_b K_d}{\theta} \qquad \text{(D-7)}$$

where R may be described statistically by an effective retardation, $\overline{R}$ = E[R], and its standard deviation, σ_R.

By analyzing the mean and standard deviation of a sample data set of a measured soil property, and by showing a relationship between the soil property and R, $\overline{R}$ and σ_R were calculated as a function of the soil property data set.

The net result of the variation in the retardation and the relationship between the retardation and ℓnK is to increase the longitudinal macrodispersivity of the sorbed species according to the following equation given by Talbott and Gelhar (1994):

$$A_{11} = A_0 \left\{ \left[1 + \gamma \frac{\sigma_R}{\overline{R}\sigma_{LnK}} \sqrt{\zeta} \right]^2 + (1-\zeta) \frac{\sigma_R^2 \lambda_n}{\overline{R}^2 \sigma_{LnK}^2 \lambda_1} \gamma^2 \right\} \qquad \text{(D-8)}$$

where A_0 is the non-reactive longitudinal macrodispersivity, λ_1 is the horizontal correlation scale, $\lambda_n \approx \lambda_1$, and γ is defined as the ratio of harmonic to geometric mean for unsaturated K.

Equation (D-8) is identical to that in Talbott and Gelhar (1994), except that the appropriate variables are evaluated for unsaturated conditions. Equation (D-8) assumes random K_d but constant bulk density and moisture content. However, using the more general case (p. 256, Gelhar 1993) when all three (i.e., K_d, bulk density and moisture content) vary, it was found that the contribution to equation (D-8) from variations of bulk density and moisture content were negligibly small, compared to variations of K_d.

The U LnK versus R relation for various strata are shown in Figure D-9. Results of stochastic analysis for macrodispersivity enhancement for different strata are shown in Table D-9. Note that the unsaturated K's were evaluated at -100 cm via the fitted van Genuchten-Mualem relation. The macrodispersivity enhancement, A_{11}/A_o ranges from about 1.06 for the H2 sandy sediments to about 1.12 for the H1 gravelly sand sediments.

Table D-9. Macrodispersivity Enhancement Estimates for Various Strata at the C Tank Farm [ρ_b in g/cm^3 and K_d in cm^3/g].

Strata	$\overline{K}_d$	$\sigma_{Kd}/\overline{K}_d$	$\overline{R}$	$\sigma_R/\overline{R}$	$\overline{\rho_b}$	$\overline{\theta}$	$\sigma^2_{\mathbf{LnK}}$	γ	ζ	λ_n/λ_1	A_{11}/A_o
Backfill (1)/ Plio-Pleistocene/ Ringold Sandy Gravel (5)	0.6	0	11.94	0.43	2.13	0.066	4.54	0.26	0.38	1	1.067
Sandy H2 (2)	0.6	0	14.31	0.67	1.76	0.115	4.60	0.13	0.58	1	1.063
Gravelly sand H3 (3)	0.6	0	14.34	0.50	1.94	0.086	4.95	0.20	0.42	1	1.062
Gravelly sand H1 (4)	0.6	0	11.36	0.38	2.07	0.081	3.19	0.32	0.72	1	1.120

Figure D-9. Uranium LnK versus R for (a) Backfill (1) and Plio-Pleistocene/Ringold Sandy Gravel (5), (b) Sandy H2 (2), (c) Gravelly Sand H3 (3), and (d) Gravelly Sand H1 (4) at the C Tank Farm.

(a)

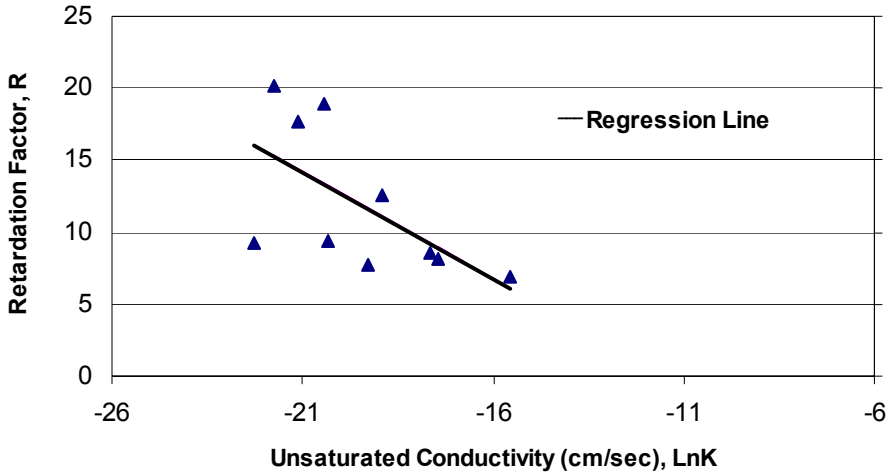

(b)

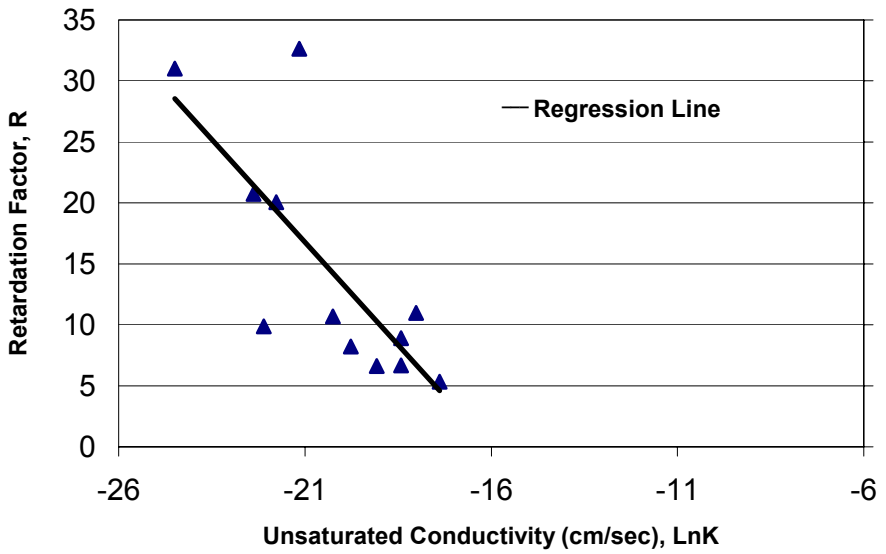

(c)

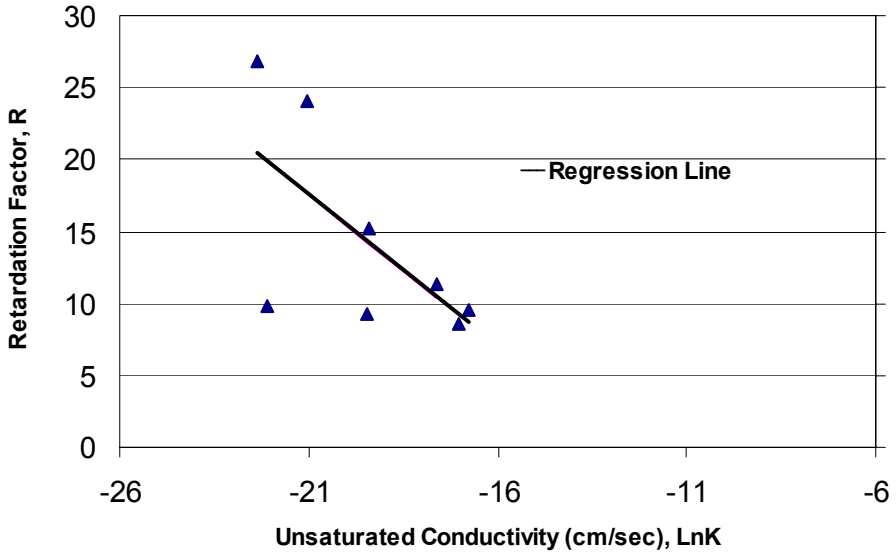
30
25
20
15
10
5
0
Retardation Factor, R
Regression Line
-26
-21
-16
-11
-6
Unsaturated Conductivity (cm/sec), LnK

(d)

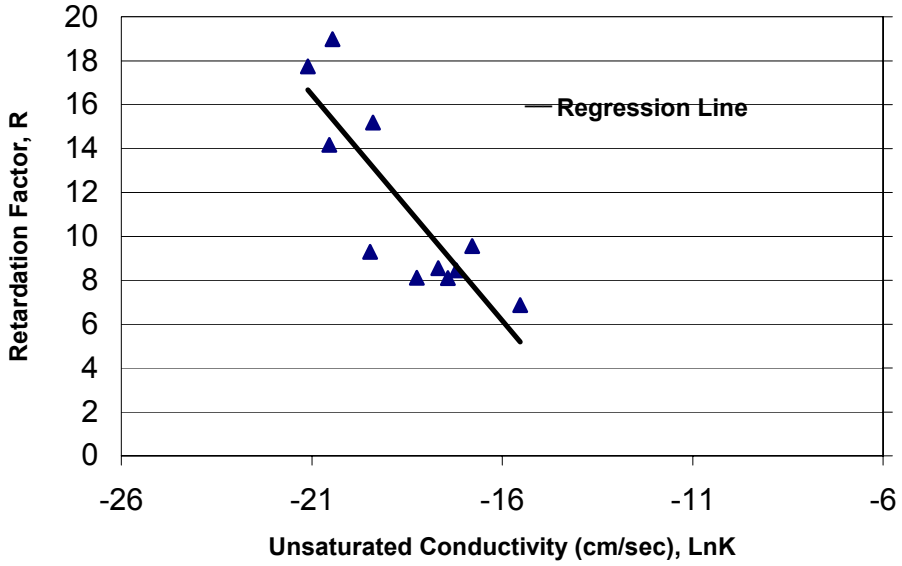
20
18
16
14
12
10
8
6
4
2
0
Retardation Factor, R
Regression Line
-26
-21
-16
-11
-6
Unsaturated Conductivity (cm/sec), LnK

3.0 REFERENCES

Bear, J., C. Braester and P. C. Menier, 1987, "Effective and Relative Permeabilities of Anisotropic Porous Media," *Transport in Porous Media,* Vol. 2, pp. 301-316.

Dagan, G., 1984, "Solute Transport in Heterogeneous Porous Formations," *J. Fluid Mech,* Vol. 145, pp. 151-157.

Freeze, R. A. and J. A. Cherry, 1979, *Groundwater*, Prentice-Hall, Inc., Englewood Cliffs, NJ.

Garabedian, S. P., D. R. LeBlanc, L. W. Gelhar, and M. A. Celia, 1991, "Large-Scale Natural-Gradient Tracer Test in Sand and Gravel, Cape Cod, Massachusetts: 2, Analysis of Tracer Moments for a Nonreactive Tracer," *Water Resources Research*, Vol. 27(5), pp. 911-924.

Gardner, W. H., 1986, Water Content, in *Methods of Soils Analysis, Part I*, edited by A, Klute, Amer. Soc. of Agron., pp. 493-544

Gardner, W. R., 1958, "Some Steady-State Solutions of the Unsaturated Moisture Flow Equation with Applications to Evaporation from a Water Table," *Soil Sci.* Vol. 85, pp. 228-232.

Gelhar, L. W., M. A. Celia and D. McLaughlin, 1994, *Modeling Field Scale Unsaturated Flow and Transport Processes*, NUREG/CR-5965, Nuclear Regulatory Commission, Washington, D.C.

Gelhar, L. W., C. Welty, and K. R. Rehfeldt, 1992, "A Critical Review of Data on Field-Scale Dispersion in Aquifers," *Water Resources Research,* Vol. 28, pp. 1955-1974.

Gelhar, L. W., 1993, *Stochastic Subsurface Hydrology*, Prentice Hall, NY.

Gelhar, L. W. and C. L. Axness, 1983, "Three-Dimensional Analysis of Macrodispersion in a Stratified Aquifer," *Water Resources Research,* Vol. 19, pp. 161-180.

Green, T. R. and D. L. Freyberg, 1995, "State-Dependent Anisotropy:Comparisons of Quasi-Analytical Solutions with Stochastic Results for Steady Gravity Drainage," *Water Resources Research,* Vol. 31, pp. 2201-2212.

Hills, R. G., P. J. Wierenga, D. B. Hudson, and M. R. Kirkland, 1991, "The Second Las Cruces Trench Experiment: Experimental Results and Two-Dimensional Flow Predictions," *Water Resources Research,* Vol. 27, pp. 2707-2718.

Kaplan, D.L. and R.J. Serne, 1999, *Geochemical Data Package For the Immobilized Low-Activity Waste Performance Assessment,* PNNL – 13037, Pacific Northwest National Laboratory, Richland, WA.

Khaleel, R. and J. F. Relyea, 1997, "Correcting Laboratory-Measured Moisture Retention Data for Gravels," *Water Resources Research,* Vol. 33, pp. 1875-1878.

Khaleel, R., J. F. Relyea and J. L. Conca, 1995, "Evaluation of van Genuchten-Mualem Relationships to Estimate Unsaturated Conductivity at Low Water Contents," *Water Resources Research,* Vol. 31, pp. 2659-2668.

Khaleel, R. and E. J. Freeman, 1995, *Variability and Scaling of Hydraulic Properties for 200 Area Soils, Hanford Site,* WHC-EP-0883, Westinghouse Hanford Company, Richland, WA.

Kincaid, C. T., J. W. Shade, G. A. Whyatt, M. G. Piepho, K. Rhoads, J. A. Voogd, J. H. Westsik, Jr., M. D. Freshley, K. A. Blanchard, B. G. Lauzon, 1995, *Performance Assessment of Grouted Double-Shell Tank Waste Disposal at Hanford*, WHC-SD-WM-EE-004, Rev. 1, Westinghouse Hanford Company, Richland, WA.

Klute, A, 1986, "Water Retention: Laboratory Methods," in *Methods of Soils Analysis, Part I*, edited by A. Klute, Amer. Soc. of Agron, pp. 635-660.

Klute, A. and C. Dirksen, 1986, "Hydraulic Conductivity and Diffusivity: Laboratory methods," in *Methods of Soils Analysis, Part I*, edited by A. Klute, Amer. Soc. of Agron, pp. 687-734.

Mantoglou, A. and L. W. Gelhar, 1987, "Stochastic Modeling of Large-Scale transient Unsaturated Flow," *Water Resources Research,* Vol. 23, pp. 37-46.

Mantoglou, A. and L. W. Gelhar, 1985, "Large Scale Models of Transient Unsaturated Flow and Contaminant Transport using Stochastic Methods," Ralph M. Parsons Laboratory Tech, Rpt. 299, Massachusetts Institute of Technology, Cambridge, MA.

McCord, J. T., D. B. Stephens and J. L. Wilson, 1991, "Hysteresis and State-Dependent Anisotropy in Modelling Unsaturated Hillslope Hydrologic Processes," *Water Resources Research,* Vol. 27, pp. 1501-1518.

Millington, R. J. and J. P. Quirk, 1961, "Permeability of Porous Solids," *Trans. Faraday Soc.*, Vol. 57, pp. 1200-1207.

Mualem, Y., 1984, "Anisotropy of Unsaturated Soils," *Soil Sci. Soc. Am. J.,* Vol. 48, PP. 505-509.

Mualem, Y., 1976, "A New Model for Predicting the Hydraulic Conductivity of Unsaturated Porous Media," *Water Resources Research,* Vol. 12, pp. 513-522.

Phillips, F., J. Mattick, T. Duval, D. Elmore, and P. Kubik, 1988, "Chlorine 36 and Tritium from Nuclear Weapons Fallout as Tracers for Long-Term Liquid and Vapor Movement in Desert Soils," *Water Resources Research,* Vol. 24, pp. 1877-1891.

Polmann, D. J., 1990, "Application of Stochastic Methods to Transient Flow and Transport in Heterogeneous Unsaturated Soils," Ph.D. Thesis, Massachusetts Institute of Technology, Cambridge, MA.

Russo, D., 1993, "Stochastic Modeling of Macrodispersion for Solute Transport in a Heterogeneous Unsaturated Porous Formation," *Water Resources Research,* Vol. 29, pp. 383-397.

Scanlon, B. R., 1992, "Evaluation of Liquid and Vapor Water Flow in Desert Soils Based on Chlorine 36 and Tritium Tracers and Nonisothermal Flow Simulations," *Water Resources Research,* Vol. 28, pp. 285-297.

Sisson, J. B. and A. H. Lu, 1984, *Field Calibration of Computer Models for Application to Buried Liquid Discharges: A Status Report,* RHO-ST-46P, Rockwell Hanford Operations, Richland, WA.

Stephens, D. B. and S. Heermann, 1988, "Dependence of Anisotropy on Saturation in a Stratified Sand," *Water Resources Research* Vol. 24, pp. 770-778.

Talbott, M. E. and L. W. Gelhar, 1994, *Performance Assessment of a Hypothetical Low-Level Waste Facility: Groundwater Flow and Transport Simulation*, NUREG/CR-6114 Vol. 3, U.S. Nuclear Regulatory Commission, Washington, D.C.

van Genuchten, M. Th., 1980, "A Closed-Form Solution for Predicting the Conductivity of Unsaturated Soils," *Soil Sci. Soc. Am. J,* Vol. 44, pp. 892-898.

van Genuchten, M. Th., F. J. Leij, and S. R. Yates, 1991, *The RETC code for quantifying the hydraulic functions of unsaturated soils*, U.S. E.P.A., EPA/600/2-91/065.

WHC, 1991, *Geotechnical Engineering Procedure Manual,* Vol. 1 and 2, WHC-EP-0635, Westinghouse Hanford Company, Richland, WA.

Wierenga, P. J., R. G. Hills, and D. B. Hudson, 1991, "The Las Cruces Trench Site: Characterization, Experimental Results, and One-Dimensional Flow Predictions," *Water Resources Research,* Vol. 27, pp. 2695-2706.

Yeh, T.-C. J. and D. J. Harvey, 1990, "Effective Unsaturated Hydraulic Conductivity of Layered Sands," *Water Resources Research,* Vol. 26, pp. 1271-1279.

Yeh, T.-C. J., L. W. Gelhar and A. L. Gutjahr, 1985a, "Stochastic Analysis of Unsaturated Flow in Heterogeneous Soils, 1, Statistically Isotropic Media," *Water Resources Research,* Vol. 21, pp. 447-456.

Yeh, T.-C. J., L. W. Gelhar and A. L. Gutjahr, 1985b, "Stochastic Analysis of Unsaturated Flow in Heterogeneous Soils, 2, Statistically Anisotropic Media with Variable α," *Water Resources Research* 21, pp. 457-464.

Yeh, T.-C. J., L. W. Gelhar and A. L. Gutjahr, 1985c, "Stochastic Analysis of Unsaturated Flow in Heterogeneous Media, 3, Observations and Applications," *Water Resources Research,* Vol. 21, pp. 465-471.